A STUDY OF THE (p,pn) REACTION ON 1p SHELL NUCLEI AT 46 MeV

C. A. Miller

February, 1974

A thesis submitted to
the Faculty of Graduate Studies
University of Manitoba

In Partial Fulfillment
of the Requirements for the Degree
Doctor of Philosophy

A STUDY OF THE (p,pn) REACTION ON 1p SHELL NUCLEI AT 46 MeV

by

C. A. MILLER

A dissertation submitted to the Faculty of Graduate Studies of the University of Manitoba in partial fulfillment of the requirements of the degree of

DOCTOR OF PHILOSOPHY

ABSTRACT

The (p,pn) reaction on four 1p shell nuclei, ^{6}Li, ^{9}Be, ^{13}C and ^{12}C, as well as the ^{6}Li(p,2p) reaction, have been studied at 46 MeV. The ^{6}Li(p,pn) cross section was found to be approximately four times that for (p,2p) and to have a very different angular dependence. Both reactions show the s-state admixture in ^{6}Li observed with (p,2p) at higher energies. For all of the target nuclei, the cross sections have features that cannot be fitted by a renormalized PWIA calculation. A zero range distorted wave calculation was found to be in only fair agreement with the ^{9}Be and ^{13}C data. The overall magnitudes of the results of the calculation were found to be very sensitive to the RMS radii of the bound state wave functions of the knocked-out neutrons.

ACKNOWLEDGEMENTS

I would like to acknowledge the important contributions of Dr. D.O. Wells who suggested the project and Dr. J.W. Watson who rendered valuable advice and assistance during the experimental measurements and the preparation of this thesis. Also, Dr. D.I. Bonbright suggested the ^{6}Li experiments, played an active role in the measurements and made a crucial contribution to the distorted wave calculations.

I wish to thank Mr. F.J. Wilson who had a large part in the preparation of the experimental equipment and Mr. D.J. Roberts who rendered assistance during the measurements.

I am also grateful to Dr. W.T.H. van Oers who always made every effort to be helpful when consulted.

Thanks are due to the cyclotron staff in general and, in particular, to Mr. John Bruckshaw for drafting many of the figures in this thesis.

Finally, I wish to acknowledge the financial support of the Atomic Energy Control Board of Canada.

TABLE OF CONTENTS

1. INTRODUCTICN

Reactions in which nucleons are knccked out of nuclei have been successfully used in the study of nuclear structure within the context of the single particle shell model of nuclei (J66,J73). This technique is especially well established in the reqion of relatively high bcmbarding energy above 100 MeV. In this case, simplifying assumptions can be made concerning the reaction mechanism which facilitate the extraction of unambiquous nuclear structure informaticn. As will be seen later, in practice this advantage tends to be offset by tne lower quality of experimental data attainable at these energies.

Largely for heuristic reasons, a very simple picture of one reaction mechanism, quasi-free scattering, will be summarized. The major assumptions are that the interaction between the projectile, hereafter assumed to be a proton, and the ejected nucleon is the same in the presence of the residual (core) nucleus as in free space and that the interaction between the scattering nucleons and the core can be neglected. In a kinematically ccmplete experiment, the mcmentum vectors of the two nucleons in the final state are measured, thereby determining the momentum of the core nucleus via kinematic relations. Under the above assumptions, the momentum of this particle is the same after the reaction as before and, of course, is equal and opposite to the initial momentum of the

ejected nucleon. Thus, in this simple picture, the single particle momentum wave function of the ejected nucleon can be directly determined by measuring the knock-out cross section over a suitable range of final state kinematic conditions. The expression for the cross section in this so-called Plane-Wave Impulse Approximation (PWIA) is (J70)

$$\frac{d^3\sigma}{d\Omega_1\, d\Omega_2\, dE_1} = PSF \quad \frac{d\sigma}{d\Omega}\Big)_{12} \quad \left|\phi(K)\right|^2 \qquad 1.1$$

where PSF is a factor involving kinematics and phase space density, $\frac{d\sigma}{d\Omega}\Big)_{12}$ is the cross section for the scattering of protons on the ejected nucleon evaluated in their centre of mass, ϕ is the bound state momentum wave function of the ejected nucleon and $-\hbar\underline{K}$ is the momentum of the residual nucleus.

The quasi-free process described by the above assumptions can be illustrated by means of a Feynman diagram (S66). Since this type of process occurs most readily on the periphery of the nucleus, the corresponding diagrams are called peripheral diagrams. Figure 1.1 shows the diagram for the knock-out of a nucleon "n" from a target nucleus "A" by a proton "p" leaving a residual core "C".

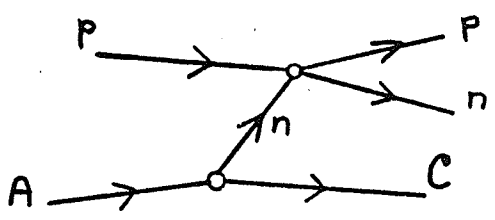

Figure 1.1: The Peripheral Diagram for a Nucleon Knockout Reaction

At the vertex on the lower left, the nucleus A emits a virtual n which then interacts with the incident p at the top vertex. The amplitude for this diagram involves the product of the amplitudes for each of the two vertices. That for the lower vertex gives rise to the third factor in formula 1.1 representing the momentum distribution of the virtual n. The amplitude for the upper vertex is that for off-mass shell proton-nucleon scattering. It is off the mass shell because the energy by which the nucleon is bound to the core causes the total energy in the centre of mass of the scattering nucleons to be smaller in the final state than in the initial state. This amplitude has been approximated in the second factor of formula 1.1 by the experimental on-shell amplitude.

Expressing the cross section in this manner further implies that there are no other competing diagrams making a significant contribution. This is clearly not the case. There are lower order processes such as elastic and inelastic scattering which may be considered to be removing incident flux. As well, there are other second-order diagrams yielding the same particles in the final state as in the quasi-free process shown above. Some of these are experimentally distinguishable from quasi-free scattering in that they selectively populate distinctive regions of final state phase space. An example is the so-called sequential process of figure 1.2 in which there is formed an intermediate excited state of the nucleus A. Such a process is recognizable through the fact that the energy of particle p is fixed for any particular

scattering angle.

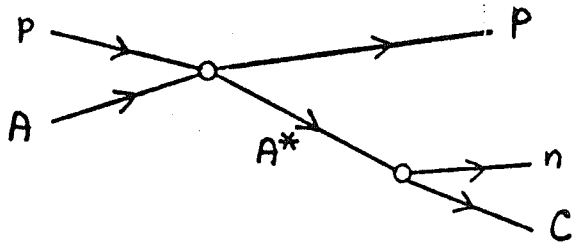

Figure 1.2: The Feynman Diagram for a Sequental Reaction

Higher order diagrams have also been found to be significant in some cases. They are probably responsible for the large differences between the cross sections for D(p,2p)n and D(p,pn)p (P70,P71).

Notwithstanding that its assumptions are clearly invalid even at high energies, the PWIA has remained a useful model. This is probably due to the fact that the most important discrepancy between its predictions and experimental results is attributable to the absorptive effects of the core. Often the most noticeable of these effects is an overall reduction in the observed cross section while, in other respects, there is fair agreement with the PWIA in the region of phase space appropriate to quasi-free scattering.

It is straightforeward in principle to approximate in calculations the diffractive and absorptive effects of the core nucleus through the use of optical model wave functions in place of plane waves. However, it has been inferred from a study of the (p,2p) reaction at 50 MeV on several 1p shell nuclei (J71) that, to a degree proportional to the binding

energy of the ejected proton, another effect of the presence of the core is important and difficult to include in calculations. At this energy, the distortions cause the knock-out cross secton to be sensitive to properties of the nucleon-nucleon interaction not determinable from two body scattering (off-energy-shell effects). Consequently, present reaction theories appear inadequate with respect to the knock-out of all but very lightly bound nucleons. Available target nuclei having such valence protons are very scarce.

It happens that there are three 1p shell nuclei with relatively lightly bound valence neutrons. These nuclei and the respective binding energies are: ^{6}Li 5.66 MeV, ^{9}Be 1.66 MeV, and ^{13}C 4.95 MeV. It was decided to undertake a study of these targets using the (p,pn) rection at 46 MeV in spite of the additional experimental difficulties in order to explore the possibility of obtaining nuclear structure information through the application of available reaction theories. The (p,pn) reaction is one of the few available tools for investigating the properties of individual neutron subshells. Also, since there has been almost no investigation of the (p,pn) reaction on nuclei other than deuterium, it was considered of interest to compare (p,2p) and (p,pn) measurements on nuclei which are expected to have structures similar with respect to protons and neutrons. One such nucleus is the above-mentioned ^{6}Li and another is ^{12}C. Because the latter has such a large neutron seperation energy (18.72 MeV), the cross section is expected to be too small to permit an extensive study. However, the (p,2p)

reaction on ^{12}C has already been measured (P67) so it was desirable to perform the (p,pn) measurement for at least one of the same angle pairs.

2. THE MEASUREMENTS

Reactions in which a nucleon is knocked out of a nucleus result in a three-body final state. One of these bodies, the residual nucleus, may be left in an excited state. In the present work, the final state was completely determined kinematically by measuring the energies and direction vectors of the two nucleons. These quantities determine through momentum and energy conservation the momentum of the residual nucleus which is of prime interest as discussed previously. Then, with all three kinetic energies known, the Q-value of the reaction and hence the excitation energy of the residual nucleus can be calculated. This degree of kinematic determination of the final state is illustrated by the fact that, on a diagram whose axes represent the energies of the detected particles at a particular pair of angles, events in which the residual nucleus is left in a given state will lie on a characteristic line, hereafter referred to as a "kinematic locus".

An important experimental parameter is the resolution with which the recoil momentum is determined. In the current experiment, the primary contribution to this resolution is from the finite solid angles subtended by the detectors. Of course these are made as large as possible without incurring a momentum resolution that would obscure information about the momentum distribution of the recoil nucleus. The effects of

finite resolution are particularly significant near zero momentum since, in a kinematic situation where zero momentum is obtained at the central or nominal values of all measured angles, all departures from these values will increase the actual momentum. It follows that a distribution which has a minimum at zero momentum will appear "filled in". The recoil momentum resolution resulting from detector solid angles typical of those used in the present work was calculated using a code called MOMERATH (W69) in order to confirm that there would not be excessive distortion of momentum distributions that could be expected from the target nuclei being considered.

CHOICE OF GEOMETRIES

Aside from a plethora of recent work on deuterium, most nucleon knock-out reaction measurements have been of angular correlation distributions with the final state nucleons having equal energies and angles. This is a tradition inherited from early work at high energies (T66,G62) using magnetic spectrometers which were not appropriate for recording energy spectra. This tradition was consolidated by the fact that the most prominent theoretical calculations using distorted waves (L66) were also restricted to this type of final state. However, incident energies below 50 MeV permit the use of solid state charged particle counters so that at each angle pair, complete correlated energy spectra may be easily recorded. This makes necessary a choice between acquiring energy spectra with good statistics at relatively few angle pairs or with

necessarily poorer statistics at a larger set of symmetric angle pairs. Data acquired via the latter scheme can be compared with the calculations mentioned above by integrating each energy spectrum over a small region about the point of equal energy sharing. Unfortunately, this means that most of the information inherent in the shape of these spectra is discarded so that experimental time is less effectively used. Furthermore, the existing theoretical codes for analysis of (p,2p) data are inapplicable to the (p,pn) reaction. The redevelopement of such a code could include a generalization to any final state kinematic configuration.

In view of these considerations, it was decided to acquire energy correlation spectra at each of several asymmetric quasi-free angle pairs as well as at a few symmetric angle pairs both more forward and backward than the symmetric quasi-free angles. The term "quasi-free angle pair" here refers to those angle pairs at which there exists a point in the energy spectrum where the momentum of the recoil particle in the final state is zero. At an incident energy as low as 50 MeV, these angle pairs are closely approximated by the possible two-body final state angles for the reaction heuristically described as nucleon-nucleon inelastic scattering with a negative Q-value equal to that of the knock-out reaction studied. Of course, the reason for choosing quasi-free angle pairs is that, at each of them, a distribution in recoil momentum is obtained which extends down to zero. Thus, the acquisition of energy correlation spectra at several quasi-free

angles furnishes information that is considerably redundant in some sense. It is reasonable to hope that this will be helpful in sorting out the effects of complexities in the reaction mechanism from manifestations of the structure of the target nucleus.

CHOICE OF BEAM ENERGY

Analysis of the data was expected to involve the impulse approximation, the validity of which is known to improve as the incident energy increases. Therefore, the experiments were performed at the highest energy, 46 MeV, at which the University of Manitoba sector-focussed cyclotron could produce a proton beam of sufficient intensity (approximately 50 na. of momentum-analyzed beam). In addition, during the ^{6}Li(p,2p) measurements, sufficient experimental time was available to acquire data at 38 MeV in order to investigate the energy dependence of this cross section.

CHOICE OF BEAM CURRENT

The magnitudes of the cross sections measured in the present work fall in the range of 40 to 200 μb/(sr^2 MeV). Consequently, the dominant contribution to uncertanties in the relative values of the measured cross sections is statistical. The experimentally measured parameter is the rate at which two nucleons in the final state are detected in coincidence. Since in the present work the rate of chance coincidences was significant in comparison, an independent sample of chance

coincidences was simultaneously recorded and subsequently subracted. The statistical uncertainty in the result is a function of both the reaction and chance coincidence rates. The properties of this function need be considered in the choice of experimental parameters such as beam current.

Let N_R and N_C be respectively the average expected values for the number of reaction and chance coincidence events recorded in any particular region of final state phase space during a measurement of time length T. Then $N=N_R+N_C$ events will be intermixed as one direct result of the measurement from which are subsequently subracted N_C independently recorded events constituting the sample of chance coincidences. The statistical uncertainty in this difference will be $\sqrt{N+N_C}$ so that the fractional uncertainty in the measurement of N_R is

$$\ell = \frac{\sqrt{N+N_C}}{N-N_C} = \sqrt{\frac{1}{N_R} + \frac{2N_C}{N_R^2}}$$

Now $$N_R = \frac{d^3\sigma}{d\Omega_1 d\Omega_2 dP} P\Omega_1\Omega_2 t b T = k_R b T$$

and $$N_C = \frac{d\sigma}{d\Omega}\Big)_1 \frac{d\sigma}{d\Omega}\Big)_2 \Omega_1\Omega_2 2\tau t^2 b^2 T$$

where b is the beam current during the measurement (assumed constant), k_R is the product of P, the phase space volume, $\frac{d^3\sigma}{d\Omega_1 d\Omega_2 dP}$ the reaction cross section, Ω_1, Ω_2 the detector solid angles, and t, the target thickness, τ is the coincidence resolving time and $\frac{d\sigma}{d\Omega}\Big)_1$ and $\frac{d\sigma}{d\Omega}\Big)_2$ are the sums of the cross sections for all reactions producing counts in the respective detectors. Thus

$$\epsilon = \sqrt{\frac{1}{k_R b T} + \frac{4\tau \left(\frac{d\sigma}{d\Omega}\right)_1 \cdot \left(\frac{d\sigma}{d\Omega}\right)_2}{p^2 \Omega_1 \Omega_2 T \left(\frac{d^3\sigma}{d\Omega_1 d\Omega_2 dP}\right)^2}}$$

The second term can be considered to be the contribution from the chance coincidences. Probably the most significant (and least universally recognized) point about this term is that it is independent of beam current notwithstanding that the ratio of chance to reaction coincidences may be made arbitrarily large by increasing the beam current. Of course, the latter has the benefit of decreasing the other term. However, even if unlimited beam intensity were available, it is otherwise limited by the count rate capability of present charged particle detection systems. The charge collection time for the type of 5 mm. thick silicon detectors used in this work is of the order of 100 ns. Significant loss of energy resolution will be incurred if the time constants of the associated pulse-shaping amplifier are not large in comparison with this value. One reason for this is that the charge collection time is a function of the spatial distribution of the released charge carriers in the detector. Pulses generated by the shaping amplifier that are seperated in time by less than their zero-to-peak rise or fall time, whichever is larger, suffer a loss of pulse height information and so must be detected and prevented from contributing to the result of the measurement if their rate of occurence is significant. From the fact that the time distribution of the pulses is described by Poisson statistics, it follows (E55) that the fraction of pulses that are "piled-up" is $2Tn$ where T is the

above-mentioned minimum allowable time seperation and n is the counting rate. (Note that this accounts for the elimation of two pulses per pile-up occurence; the pile-up rate is Tn^2). For each charged particle detection system, both the total number of pulses, N, and the number of pile-ups, N_p, must be counted during the measurement and used tc correct the data for the losses by dividing the result by $1-2N_p/N$. It is clear that there is no point in employing a beam current higher than that which yields an overall piled-up fraction of 50%.

PULSE PROCESSING POLICY

A common feature of all measurements was that as much information processing as possible was done with the on-line computer rather than by special purpose electronic circuits. Essentially all pulse height information was digitized and logged on magnetic tape as well as prccessed for the purposes of on-line displays and plots. It was also possible to use the results of the online processing to restrict the logging process to specific catagories of events in order to prevent the recording of excessive amounts of data from extraneous events. Examples of the online processing done was the discrimination of protons frcm other charged particles and of neutrons from gamma rays. This was repeated in a more comprehensive form as part of the off-line reduction of the logged data.

TARGETS

The ^{6}Li targets were self-supporting foils of thickness approximately 8 mg/cm^2 and isotopic purity 99.3%. They were prepared by pressing a lump of the metal between two flat tool-steel surfaces using a force of approximately 40 tons. During this process, the lithium was kept wet with oil to prevent oxidation. It was necessary to place layers of .001 inch polyethylene film between the steel surfaces and the lithium in order that they be separable after pressing. Even though much of the polyethylene flowed out under pressure, enough remained to accomplish its purpose. The following steps were taken to prevent oxidation during transfer of the targets to the scattering chamber. The chamber or target lock, as the case may be, was evacuated and vented to argon gas. This permitted the top to be removed for a few minutes without admitting a significant amount of air in the region of the target ladder. A beaker of trichlorethylene was lowered into the argon atmosphere and the target which had been mounted on a frame while still wet with oil, was washed in the solvent to remove the oil and then quickly mounted on the target ladder. The chamber was then evacuated immediately.

Each target's thickness was determined by measuring the elastic scattering cross section at a few scattering angles using the same detectors as in the correlation cross section measurement. The values obtained were normalized to published cross sections (B72). Since the same angles and beam energy were used for these purposes during both the (p,2p) and (p,pn)

measurements, errors in the published data would not be reflected in the ratio of the (p,2p) tc (p,pn) cross sections.

The ^{9}Be and ^{13}C targets were ccmmercially obtained (E72,P72) self-supporting fcils of respective thicknesses 4.7 and 7.0 mg/cm^2. The latter was isotcpically enricned to 95.7%. Since the neutron separation energy for ^{12}C is about 14 MeV greater than that for ^{13}C, there was no difficulty in eliminating the contribution of the fcrmer.

A method used by Pugh et. al (P67) was followed in the preparation of the ^{12}C target foil. Several layers of filter paper of low ash content normally used for quantitative analysis were charred in a vacuum while pressed between quartz plates to prevent wrinkles from developing. The temperature was slowly raised to cherry redness over a period of approximately half an hour and left there for about an hour. Non-uniform shrinkage and the conseguent probability of tearing was avoided by heating uniformly over the whole surface. The result of this method was a satisfactorily rugged foil. Its thickness of 8.86 mg/cm^2 was determined by weighing a known area.

THE ^{6}Li(p,2p) EXPERIMENT

The proton knockout experiment was performed in a 28 inch diameter precision scattering chamber. It is located in the beam line labelled "45° right line" on figure 2.1 which shows the layout of the experimental area. The mcmentum analysis afforded by the 45° bend in the switching magnet yields a beam energy spread of 150 KeV. On this beam line, the energy of the

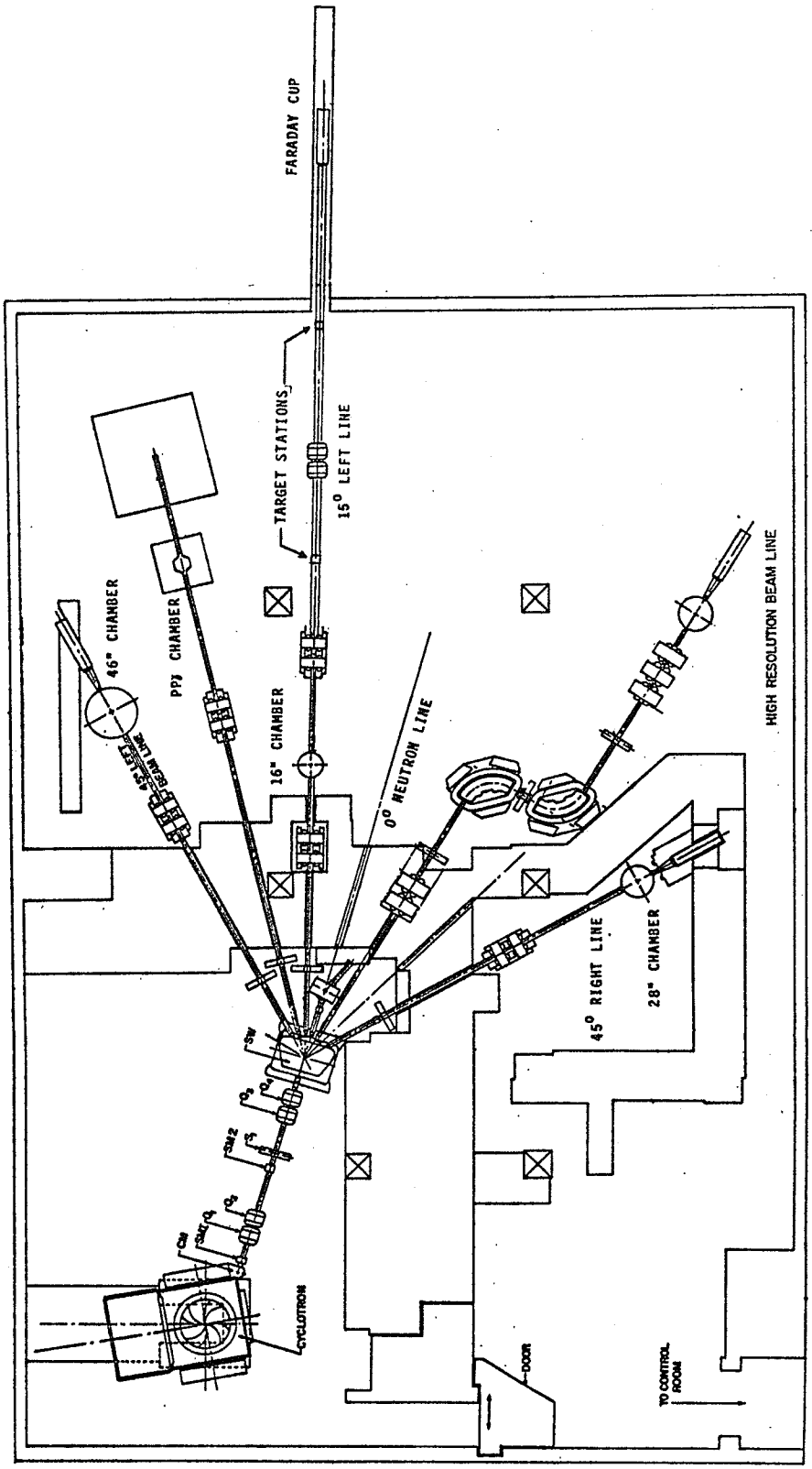

Fig. 2.1 Layout of University of Manitoba cyclotron experimental area.

beam is determined through measurement of the magnetic field in the switching magnet by the nuclear magnetic resonance technique. The relaticnship between the magnetic field and the beam energy had previously been calibrated using the "cross-over" method (B64).

The 28 inch scattering chamber has two independently-rotatable freon cooled detector platforms. On each of these was mounted a detector telescope consisting of a 200 micron thick "delta E" silicon surface barrier detector followed by a 5 mm. thick lithium-drifted silicon "E" detector and a "veto" detector. The collimators subtended vertical and horizontal angles of 4.6° and 2.3° respectively. For each of the two telescopes, the relationship between the energy deposited in the "delta-E" and "E" detectors was used in the identification of the detected particles. The presence of a signal from the veto detector indicated that the energy of the particle was above the range of interest and so was used to inhibit the recording of the event. This information could have been gleaned from the energy lost in the first two detectors had such events been recorded but this would have unnecessarily increased the computational load on the computer as there was a relatively large count rate of high energy elastically-scattered protons in chance coincidence. Timing information for the implememtation of the fast coincidence requirement was derived from the delta-E detectors. Their relatively large area of 200 mm^2 and small thickness were chosen to respectively minimize radiation damage and maximize

the energy range of identifiable protons. However, both these characteristics reduce the effective signal to noise ratio with respect to time resolution so that special measures were necessary to reduce the effects of r.f. noise generated by the cyclotron.

A block diagram of the electronics is shown in figure 2.2. All modules were obtained commercially. The main pulse shaping amplifier employed gaussian active-element shaping techniques with time constants of .5 microseconds which permitted pulse rates of over 50 KHz. Their outputs passed through d.c.-coupled amplifiers into the base-line restored inputs of the ADC linear gates which were opened by the fast coincidence condition. The output of the charge sensitive preamplifiers for the delta-E detectors were also passed through a d.c.-coupled wide band amplifier whose output impedance was modified to match as closely as possible the 50 ohm cable attached so that reflections arriving back at this output were completely absorbed. This was in order that a shorted length of cable whose delay was equal to 3/2 r.f. periods could be attached at the high-impedance input of the next amplifier so that r.f. noise was cancelled by the reflection at this point. The cable delay was long enough so that there was no effect on the leading edge of the pulses. Timing information was derived from the pulses by means of a combination of timing-filter amplifiers which provide an adjustable band-pass and constant-fraction-of-pulse-height discriminators. The fast coincidence requirement was implemented with a

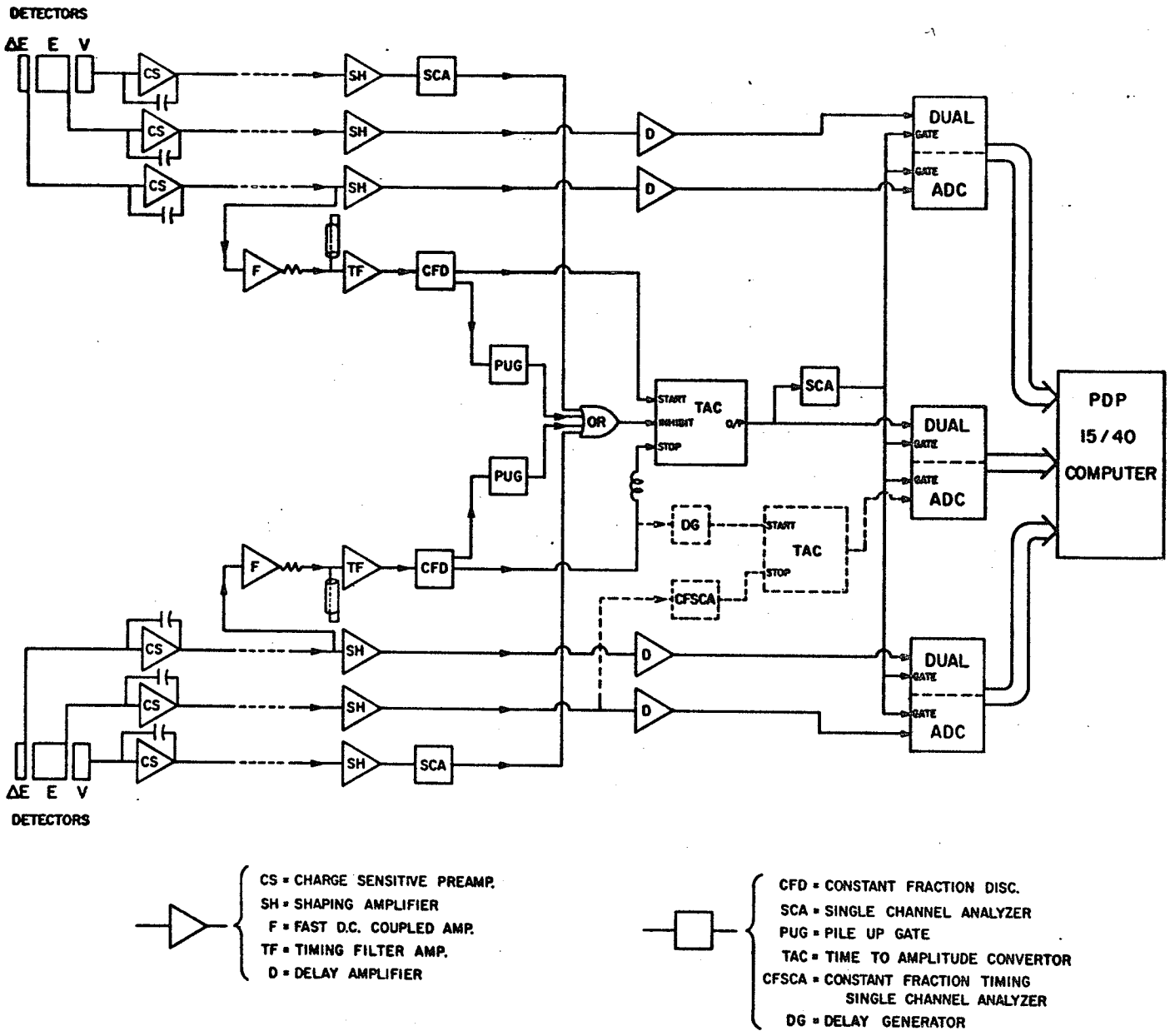

Fig. 2.2 Schematic of electronics used for (p,2p) measurements.

time-to-pulse-height convertor (TAC) whose output was digitized and recorded by the computer so that long term timing drifts could be noted and accomodated during data reduction. A time resolution well within the beam burst separation was obtained. As explained previously, the data acquisition rate was limited by the piling-up of pulses in the shaping amplifiers so that it was necessary to detect and discard events involving these occurrences. This was done for each detector telescope by a pile-up gate which generated an output used for inhibiting or resetting the TAC whenever two input pulses arrived within 3 microseconds of one another. Both the total number of input and output pulses of the pile-up gate were scaled so that the previously-mentioned correction could be applied during data reduction. The TAC was also inhibited by the detection of any particle in the veto detectors.

During one experimental run, it was found that one 5 mm. Si(Li) detector produced substandard signals for a very small fraction of particles stopping in it. The fraction was small enough that the loss of events was negligible. However, the cross section for the ^{6}Li(p,pd) reaction is many times that for ^{6}Li(p,2p). The faulty detector caused some deuterons to be mis-identified as protons and simultaneously changed the final state kinematics to match those of a (p,2p) reaction. Fortunately it was possible to eliminate the contaminating events by effectively measuring the charge collection time in the detector. The method used was a form of pulse shape discrimination. The output from the corresponding shaping

amplifier was applied to a constant-fraction-of-pulse-height single channel analyzer which triggers on the trailing edge of the pulse. An additional TAC was used to record the time of its output relative to the previously-discussed fast timing signal from the delta-E detector in that telescope. The correlation between this TAC output and the energy recorded in the faulty detector revealed a distinct characteristic of the invalid events which could be used to eliminate them. Since this restriction was applied in the form of a veto, there was no risk of losing valid events through less than 100% efficiency of the single channel analyzer which was operating at a high count rate.

Typical measurement periods for one angle pair were about 4 hours. This provided approximately 7% statistical accuracy for the typical cross section of .04 mb/(sr²MeV).

THE (p,pn) MEASUREMENTS

Experiments involving the detection of uncharged neutrons pose many problems not encountered with charged particles. The neutron's energy is measured through its time of flight so that a major effort is usually required to obtain the best time resolution possible. Detection of the neutron is accomplished indirectly through its interaction with nuclei in an organic scintillator; hence the efficiency of the detector is much less than unity and is a function of neutron energy. This means it must be obtained by direct measurement or sophisticated calculations involving various assumptions. Finally, there is

the ditficulty in avoiding the detection of neutrons generated by reactions occuring other than in the target. For example, the beam dump usually produces a neutron flux several orders of magnitude larger than that from the target. In a correlation experiment such as (p,pn), this flux will contribute only to the chance coincidence rate but, in the present case, the contribution to the total experimental uncertainty from the randoms was significant.

Beam Transport

Background flux was minimized by the design of the beam line used for the (p,pn) measurements. It is labelled "15° left line" in figure 2.1. After passing through the target in the "16 inch chamber", the beam was transported across the underground room by another quadrupole doublet into a hole extending approximately 8 m. into the wall and the clay behind it. The Faraday cup for stopping and measuring the total charge of the beam flux was located approximately 5 m. into the wall, the remaining space allowing the predominantly forward-directed flux to proceed as far as possible from the opening in the wall before encountering material from which it could back-scatter. It was found that there was a significant "halo" to the beam which generated background when in collision with the beam pipe. To minimize the effects of this, 6 inch beam pipe was used after the quadrupole doublet immediately downstream from the 16 inch chamber. In addition, a special section of pipe was constructed to closely fit the pole faces of the 4 inch

quadrupole magnets. The latter provision accomodated the temporarily defocussing effect of the first quadrupole in the doublet. By comparing the beam current in the Faraday cup with that measured on a screen upstream from the scattering chamber, both with and without a ^{12}C target in position, it was ascertained that multiple scattering by the target caused a loss in beam transmission of less than 2%.

Because the beam is bent through the relatively small angle of 15° in the beam switching magnet, the momentum analysis yields an energy spread of approximately 400 KeV in this beam line. However, this is adequate for many knockout reaction studies.

The beam spot at the target position was contained within an area 1/8 inch wide by 1/4 inch high. Since this was smaller than the proton detector aperture, its contribution to the overall angular resolution was less important.

The Scattering Chamber

The 16 inch scattering chamber (shown in figure 2.3) was designed to have as low a mass as possible to minimize the scattering into the detector of neutrons produced in the target. To obviate corrections for neutron attenuation and to permit the detection of charged particles outside the chamber at almost any scattering angle, the wall of the chamber in the scattering plane consisted of "Kapton-H" foil. The atmospheric load on the lid was supported by six pillars which could be moved to angles which caused the least interference to the

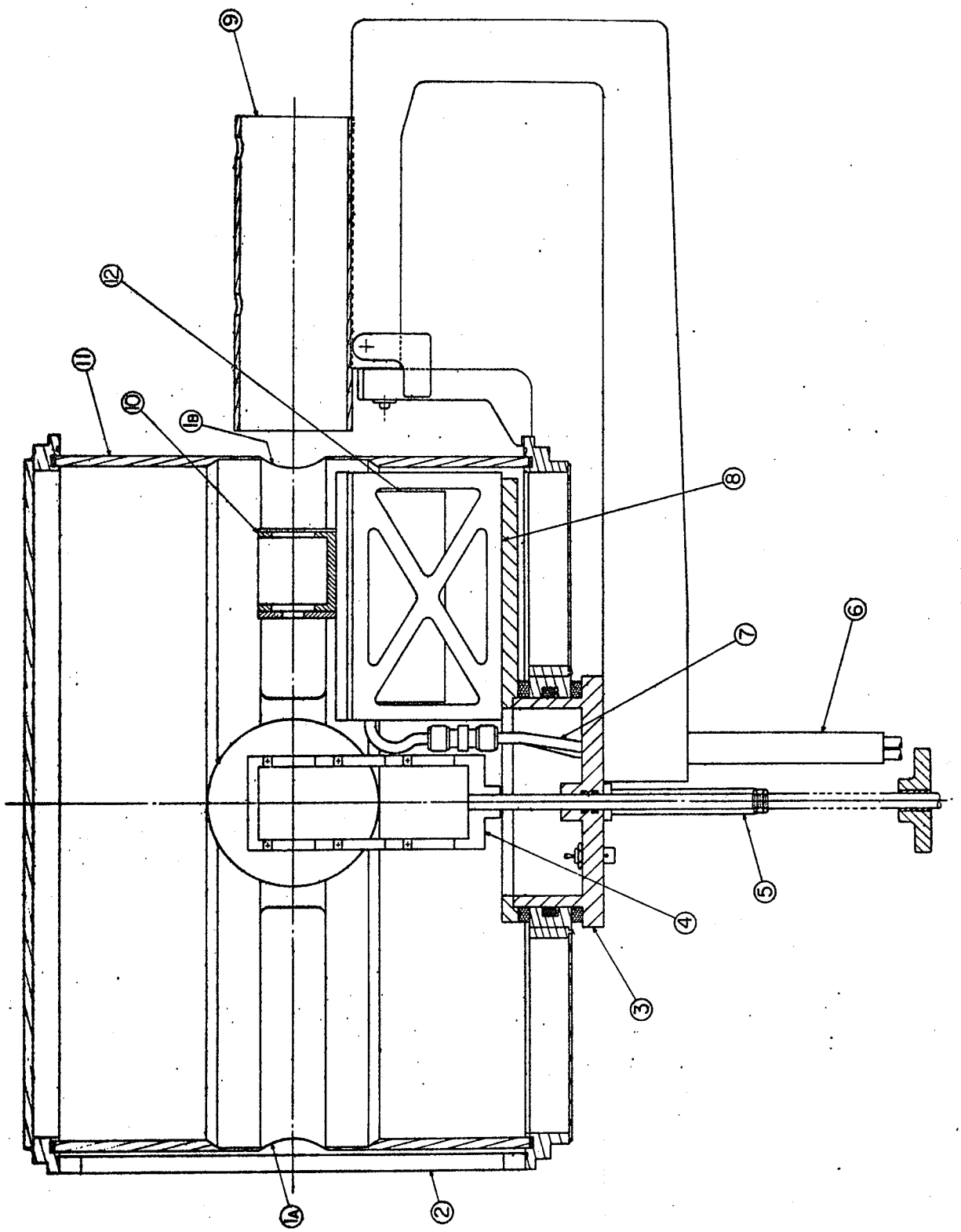

Fig. 2.3 A cross section of the 16 inch scattering chamber used for the (p,pn) measurements. The labelled components are as follows: 1. "Kapton-H" foil of thicknesses a) .005 inches b) .003 inches. 2. Moveable pillars 3. Rotating hub for detector platform. 4. Target ladder 5. Target ladder clamp 6. Stainless steel standoff for cooling lines 7. Cooling lines 8. Nylon support for detector platform 9. Mount for NaI(Tl) detector assembly 10. Solid state detector cube 11. Aluminum wall of chamber 12. Liquid nitrogen reservoir

particular measurement being made. A cooled rotatable table for mounting solid state charged particle detectors was built into the floor of the chamber which was made rigid enough to maintain alignment under atmospheric load by a steel rib structure. Liquid nitrogen was the cooling medium. A small storage container of approximately 1/4 litre capacity was soldered to the bottom of the detector platform and was filled automatically by a level sensor inside the container. Thermal isolation together with mechanical rigidity were provided for the detector platform by a box-shaped structure of pillars and cross members machined from a single piece of nylon.

The Proton Timing Signal

The neutron time of flight was measured using the signal from one of the proton detectors as a reference as this yields better resolution and stability than the microstructure of the cyclotron beam. However, special measures are necessary to obtain this resolution without sacrificing energy resolution. Since the usual "charge sensitive" integrating preamplifiers used with solid state detectors throw away a great deal of timing information, a technique developed by Sherman, Roddick and Metz (Sh68) was adopted which employs a seperate fast voltage-sensitive preamplifier to provide the timing information. This preamp detects the voltage across the detector itself which in enhanced to a reasonable level by an inductor introduced in series with the input to the usual charge sensitive preamp so that the charge collected on the

detector is blocked with a time constant of about 100 ns. Since this is small compared to the shaping amplifier time constants, the effect on energy resolution is small. In order to minimize the capacitance in parallel with the detector, the timing preamp was mounted inside the scattering chamber and connected to the detector by only about two inches of cable. A nylon standoff between the preamp and the detector platform provided thermal insulation. This prevented the temperature of the electronic components in the preamp from falling below their operating range.

Silicon surface barrier detectors have the best timing characteristics of solid state detectors. One of these was used for this purpose. It also provided the "delta-E" signal for particle identification and the elimination of high energy protons which passed through all the detectors. The techniques used for these purposes are described later in the section "The Online Computer".

Considerations entering into the choice of the thickness of the timing detector included the following. The time resolution, r, is given by

$$r = V_N/(dV/dt)$$

where V_N is the equivalent RMS noise voltage referred to the input of the timing preamp and V(t) is the signal voltage induced by the charge collected across the detector. dV/dt is evaluated at the triggering threshold. In order to relate this to D, the detector thickness. the following approximations are made.

$$dV/dt \propto V/T$$

where V is the maximum signal voltage and T is the detector's total charge collection time. Now, in the worst case, where a high energy proton deposits the least energy in the detector,

$$V \propto dE/C \propto D^2$$

where dE is the energy lost which is proportional to D and C is the total capacitance of detector, signal lead and preamp input. If that of the detector dominates, $C \propto 1/D$. Finally, $T \propto D$ since the electric field strength that can be sustained is roughly independent of thickness. Therefore $r \propto 1/D$. However, as the thickness increases, the cost of the detector ultimately rises very quickly. Also, as the capacitance falls and becomes comparable to the stray capacitance, the improvement in resolution becomes less significant. In the present case where solid angle requirements dictated a detector area of at least 100 mm^2, these factors limited the thickness to about 750 microns.

The mobility of charge carriers in silicon increases as the temperature in reduced. Fortuitously, measurements (M69) indicate that the minimum collection time is attained at approximately the boiling point of nitrogen, 77°K. Furthermore, detector noise is reduced. Very significant improvements in time resolution were obtained in the present case by cooling the detectors with liquid nitrogen.

The Proton Detector Telescope

Either a 5 mm. Si(Li) detector or, on one occasion, a

NaI(Tl) scintillator was mounted behind the timing detector. Using only these two, no proton with an energy less than 10.5 MeV could be identified since it was stopped in the first detector. In order to include lower energy protons in the measurements, in some cases a 200 micron thick surface barrier detector was added in front of the others. This meant approximately 5 MeV protons would deposit sufficient energy in the timing detector to produce adequate time resolution. For the sake of convenience, the three detectors will henceforth be called epsilon, delta and E in physical order. All three were incorporated in particle identification using the on-line computer. The particle flux entering the detectors was collimated by a copper slit barely thick enough to stop the highest energy proton. It subtended horizontal and vertical angles of 2.4° and 4.7° respectively. A magnetic field generated by a small permanent magnet was used to prevent detector damage by the large fluxes of low energy electrons scattered from the target.

The Neutron Detector

During the early development stages, an attempt was made to use a plastic scintillator as the neutron detector. It was found that there was an unexpectedly high gamma ray background flux contributing to the chance coincidence rate and that the contribution of the latter to the total statistical uncertainty in the data could be considerable. By manipulating various forms of directional ad hoc shielding, it was deduced that much

of the background flux was isotropic in space as well as uniform in time. From the pulse height spectra, it was surmised that an important part of it was due to thermalized neutron capture by the hydrogen component of the concrete walls of the room. In view of this situation, it was considered necessary to discriminate between neutrons and gammas. Resort was made to Ne213 (N71) liquid scintillator contained in a 5 inch long by 4.5 inch diameter cylindrical capsule mounted on an RCA 4522 photomultiplier tube. Because the photocathode of the latter was operated at negative high voltage, the scintillator can was also connected to this potential to prevent possible electrolysis of the faceplate and consequent poisoning of the photocathode. The inside of the capsule was coated with isotropically-reflecting white paint. It was found that a standard technique for pulse shape discrimination which is described below provided the means of distinguishing neutrons from gamma rays.

The time resolution of these detectors proved to be significantly better than could be expected from simple considerations involving uncertainties in the neutron flight path due to the length of the scintillator. In other words, the effective speed of light in the propagation from the locality of interaction in the scintillator to the photocathode is considerably less than is expected from the index of refraction. This is probably due at least in part to the excellent reflective properties of the paint on the inside of the scintillator cans.

For some of the measurements, two of these scintillator assemblies were stacked vertically to increase the detector solid angle. Typical flight paths ranged from 3 to 4 metres. They were chosen to have the minimum lengths that would satisfy both the requirements that the neutron energy resolution be sufficient to resolve states in the residual nucleus of the reaction being studied and that the angular resolution be small enough to yield an acceptable recoil momentum resolution.

The (p,pn) Electronics

A schematic of the maximal configuration of the electronics used in the (p,pn) measurements is shown in figure 2.4. The linear pulses from the solid state proton detectors were treated in a manner similar to that already described for the (p,2p) measurements. The primary difference, already mentioned, is in the method of obtaining timing information from the delta detector. Following the voltage sensitive preamp mounted inside the chamber, the sequence of fast wide-band amplifier, r.f. clipping stub, timing filter amplifier and constant-fraction-of-pulse-height discriminator are again the same except that, in this case, the length of the stub, the time constant of the filter amplifier and the shaping delay of the discriminator were all considerably shorter. Respectively, these were 1/2 r.f. wavelength, 10 ns. differentiation and about 5 ns. The time resolution of this configuration was measured using proton-proton elastic scattering with one final state proton passing through the delta detector and the other

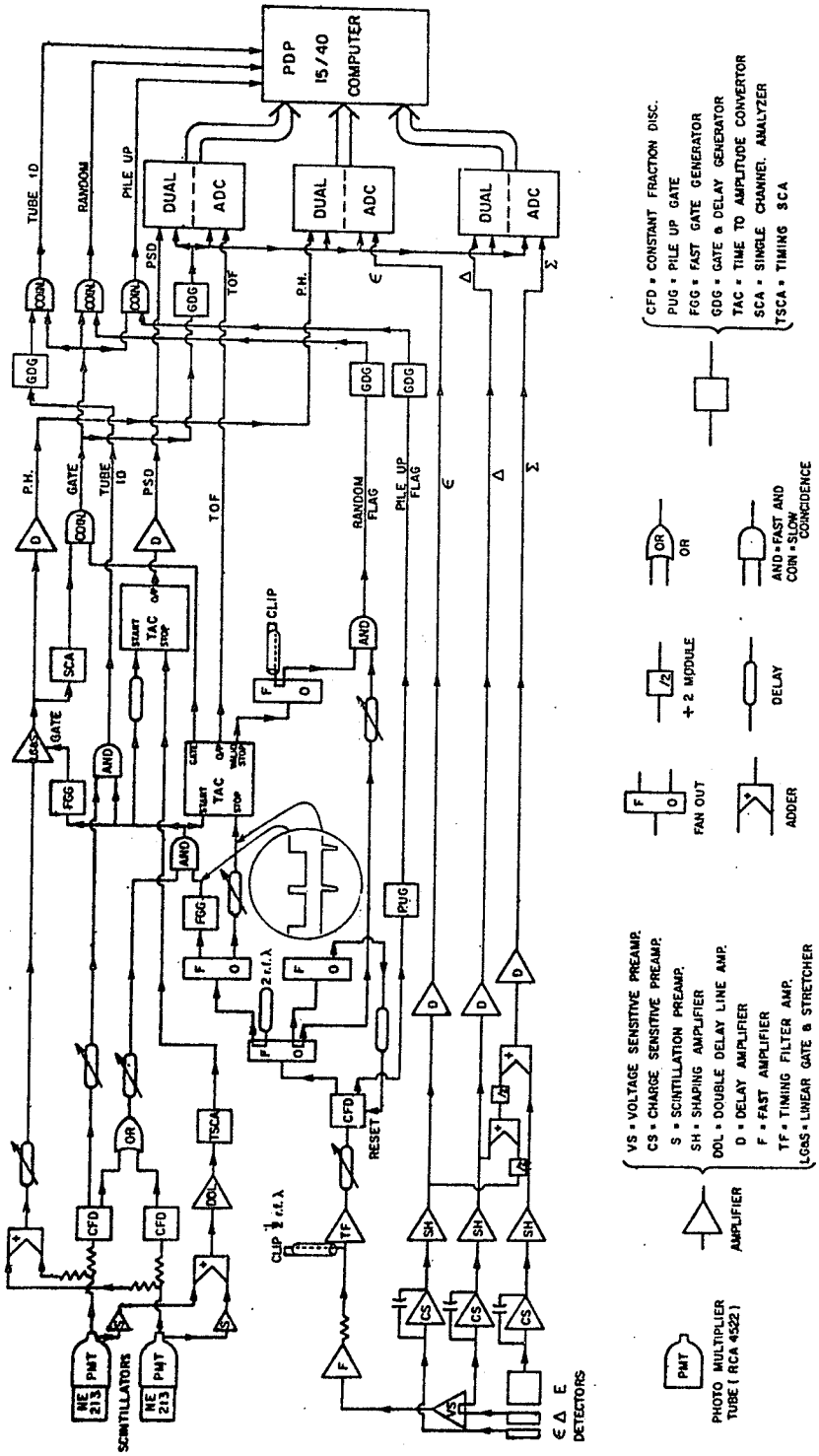

Fig. 2.4 Schematic of maximal configuration of electronics used for (p,pn) measurements.

stopping in a small plastic scintillator mounted on an RCA 8575 photomultiplier tube. Including the contribution from both detectors, the resolution was 350 picoseconds. From similar tests using two such scintillators, it was known that its contribution was smaller than that of the delta detector system. Since monoenergetic protons were used in these tests, no indication was obtained of the relative magnitude of timing "walk" (systematic variation of time as a function of pulse height). However, in a correlation experiment such as this, timing walk will only distort the energy correlation spectra in the direction of the neutron time of flight axis, which is unimportant since the final state is kinematically over-determined.

It was found necessary to deliberately incur an approximately 200 ns. period of "dead time" following each trigger of the constant fraction discriminator. This was in order to eliminate some "double pulsing" due to the complex shape of the pulses entering the discriminators. Even a small amount of double pulsing would have invalidated the operation of the pile-up gate which was used to detect and reject pulses ocurring within 3 microseconds of one another, as in the (p,2p) measurements. The dead time period resulted in approximately 7% of the pile-ups escaping detection but the pileup rate was typically less than 20% of the total counting rate in the delta detector.

A sample of chance coincidences were recorded simultaneously with the reaction data. Special precautions were

taken because the coincidence requirements and the time of flight measurement are so closely related. Chance coincidences were generated by causing each pulse from the proton discriminator to produce two pulses separated by an exact multiple of the cyclotron r.f. period. It was necessary that this separation period be longer than the range of useful neutron times of flight and that it be such a multiple because of the possibility of a cyclical variation in the intensity of the total flux arriving at the neutron detector. Four r.f. periods or 140.4 ns. was chosen for the delay. Relative delays between the two detector systems were arranged so that the second of the pair of pulses generated the reaction coincidences. This was because it was considered less likely that a proton rather than a neutron from a reaction would be inordinately delayed to the extent that it would erroneously appear in the sample of chance coincidences. The second pulse was generated by connecting to the bridged high impedance output of a logic fan-out module a precisely calibrated length of delay cable which was open at the other end. In general, long delay cables transmitting fast NIM logic pulses were constructed of RG 8/U type cable to prevent attenuation of the pulses to substandard levels.

A fast d.c.-coupled gating system was employed to "start" the TOF (time-of-flight) TAC only when an event ocurred with a time of flight in the range of interest. This not only virtually eliminated TAC dead time but also afforded convenience in that a relatively early signal was available

which indicated a valid time of flight and the time delay of which was fixed relative to the neutron detector signal. The gate producing this signal will be henceforth called the TOF gate. Its input from the proton detector was in the form of two stretched pulses seperated by the previously mentioned 4 r.f. periods. Their width determined the range of acceptable times of flight. If the pulse from a neutron detector timing discriminator fell within one of these gating pulses, it identified a chance or reaction coincidence event, respectively.

Signals were used from both the anodes and dynodes of neutron detector photomultiplier tubes. The anodes supplied both timing information and pulse heights for threshold determination. Simple resistive networks were used to split the anode signals so that 1/4 of their amplitude was gated and integrated to form the "pulse height" signal and the rest was applied to the constant fraction discriminators. "Pulse shape discrimination" for the elimination of gamma rays was performed using the dynode signals. The dynode signals of the two tubes were integrated by scintillator preamps before being mixed together and applied to the input of a double delay line shaping amplifier with a time constant of .8 microseconds. This method of pulse shape discrimination relies on the fact that a liquid organic scintillator such as that being used here produces light pulses that consist of two distinct components which decay in time with different decay constants. The relative intensity of these two components depends on the

ionization density of the charged particle to which the incident uncharged particle has transferred some of its energy. Electrons, from which gamma rays scatter, produce a lower ionization density than the protons and heavier particles through which neutrons are detected. Because the time at which the bipolar output of the double delay line amplifier crosses the baseline depends significantly on the decay constant of the tail of the pulse from the photomultiplier tube, it can be related to the type of particle detected. This crossover time was determined by a timing single channel analyser whose output was used to stop another TAC, henceforth call the PSD TAC. It was started by the TOF gate output.

The TOF gate output also opened the fast linear gate and stretcher which processed the anode pulse height information. Since the linear gate was held open for only approximately 100 ns., the number of pulses piled up was negligible so that no pileup gate was necessary for the neutron detector. The pulse height threshold was defined in terms of the slow linear signal representing the integrated anode pulse height because of the superior resolution and stability possible with slow linear systems. The trigger levels of the timing discriminators for the neutron detectors were set well below the level corresponding to the threshold of the single channel analyser following the linear gate and stretcher. This was necessary not only to insure that the constant fraction discriminators had no effect on the resultant pulse height threshold but also because they demonstrated considerable timing walk near their

thresholds.

When more than one neutron detector was used, the outputs of their discriminators were mixed before application to one input of the TOF gate. Since it was desirable to record which of the detectors had registered each event, the TOF gate output was gated with the appropriately-delayed signal from one of the discriminators thereby generating a signal called "tube id." whenever the corresponding detector generated an event. A similar arrangement was necessary to determine whether an accepted timing pulse from the neutron detectors had fallen within the reaction or chance coincidence time windows. In this case, use was made of the fact that the leading edge of the so-called "valid stop" output of the TOF TAC was time-registered on the stop input that caused the conversion. Therefore, this pulse was clipped with a shorted cable a few feet long and gated with the appropriately delayed signal from the proton discriminator. This delay was such that an overlap was attained whenever the first of the double pulses generated an event. Consequently, the resulting signal identifying chance coincidences is called the "random flag".

Altogether, six linear signals were digitized by ADC's and read into the on-line computer. These were the neutron detector pulse height and PSD TAC output, the TOF TAC output, the signals from the epsilon and delta detectors and the linear sum of the signals from all three proton detectors which was called "sigma". The linear gates internal to the ADC's were opened by a signal produced by a slow coincidence between the output of a

single channel analyzer defining the minimum neutron detector pulse height threshold and the so-called "GATE" output of the TOF TAC which, in this case, is the delayed equivalent of the TOF gate output. The neutron detector pulse height was recorded to assist in pulse shape discrimination as well as to permit either the choice of a higher threshold during off-line analysis or even a threshold which is a function of other recorded parameters although neither of these possibilities proved necessary. Three more binary bits of information were recorded with each event. These were the previously mentioned "random flag" and "tube id." as well as the indication from the pile-up gate that the proton energy measurement may have been invalidated. Of course, these three signals were gated by the condition that also opened the ADC linear gates.

Linear gain calibrations were required for both proton and neutron detectors. It was necessary that the signals being added together to form the "sigma" pulse representing the total proton energy all represented the same energy per volt. This was achieved by adjusting the gains of the shaping amplifiers until the same value of sigma was registered by the computer when the same test pulse was applied to each of the inputs of the three charge integrating preamps. Also, an absolute calibration of the energy scale was performed by recording spectra of elastic and inelastc scattering from a deuterated polyethylene target at various detector angles chosen tc provide clearly identifiable peaks in the spectra at various points in the energy range of interest.

Neutron Detector Threshold Determination

Calculation of the neutron detector efficiency requires the knowledge of the pulse height threshold in equivalent electron energy. This was obtained by recording pulse height spectra produced by gamma rays of three different energies in the neighbourhood of the threshold. The sources used and the corresponding gamma ray energies are:

^{60}Co	1.173, 1.332 MeV	(averaged)
^{212}Pb	2.61 MeV	
^{12}C bombarded by proton beam	4.43 MeV	

The dominant mode of interaction of gamma rays in organic material in this energy region is Compton scattering. According to a prescription developed empirically (E73), the maximum electron energy, which can be computed from the gamma ray energy via kinematic relations, corresponds to the point in the spectrum on the Compton edge where there are 2/3 as many counts as at the peak. A straight line was fitted to the three points derived in this way.

Neutron Detector Efficiencies

Only a fraction of the neutrons incident on the neutron detector interact with nuclei in the scintillator in a manner which is detected. This fraction, called the efficiency, depends on many parameters including the energy of the neutron, the scintillator geometry and material and the amount of light required to exceed the pulse height threshold discussed above.

Several methods of determining this efficiency have been employed. One is direct measurement using an independently-known neutron flux. Another is to calculate it using the experimentally determined cross sections for all the nuclear reactions that the incident neutron may undergo in the scintillator. Depending on the approach used, this may require a number of simplifying assumptions because of the geometrical complexities associated with multiple scattering in the scintillator. Usually these two methods are combined to the extent that the accuracy of the computer codes developed for the calculation of efficiencies is determined by comparing their predictions to some experimentally determined efficiencies. The magnitude of the discrepancies revealed is taken to be an indication of the uncertainties involved in using the code in the measurement of unknown cross sections.

The efficiencies for the present measurements were computed using a code (S71) employing a Monte Carlo technique for the simulation of scattering histories in the scintillator of a large statistical sample of incident neutrons. This approach obviates the need for many of the above-mentioned simplifying assumptions. The code has predicted efficiencies that are typically within 5% of measured values. Figure 2.5 shows the computed efficiency as a function of incident neutron energy of the scintillators used in the present measurements for two different pulse height thresholds. Curve A corresponds to the threshold used for the $^{12}C(p,pn)$ measurement while curve B was used for the $^{13}C(p,pn)$ work. Different thresholds were

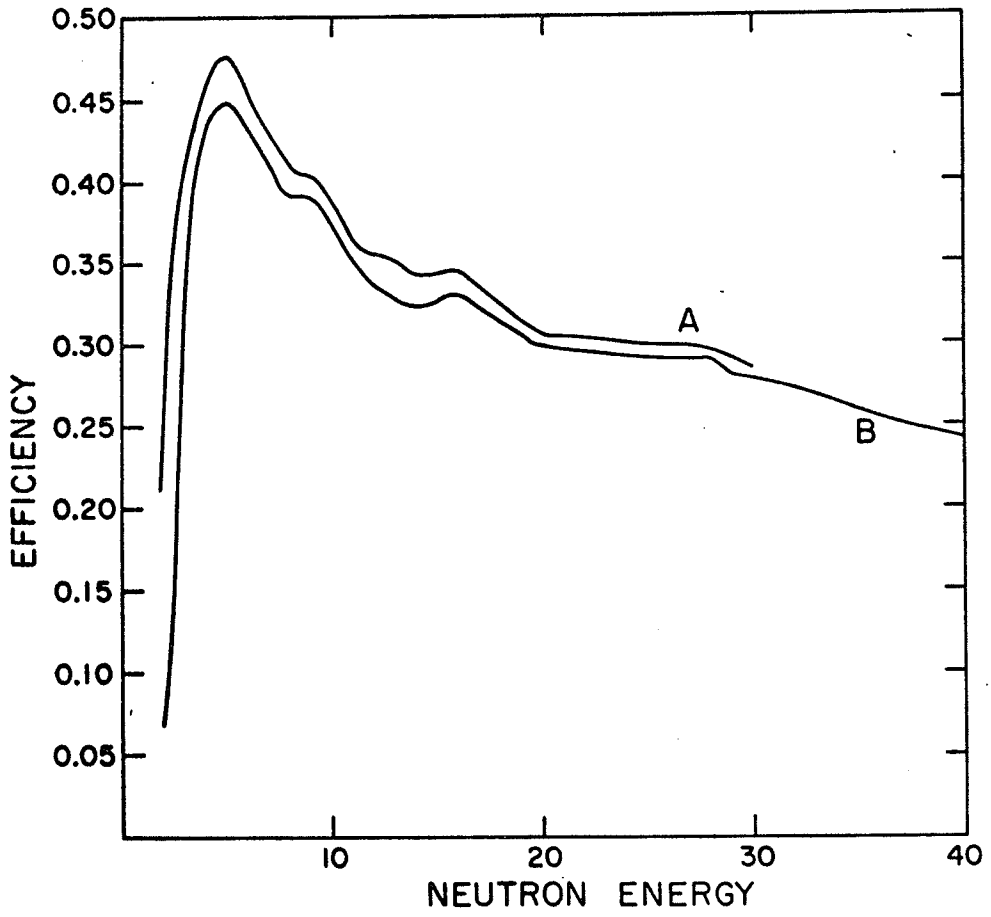

Fig. 2.5 Neutron detector efficiencies computed by the Monte Carlo technique. Curve A is the average of the efficiencies for the two thresholds of 0.27 and 0.40 MeV while curve B is the average of those for 0.42 and 0.50 MeV equivalent electron energy.

used for these reactions because their Q-values are so different.

Beam Energy Measurement

The energy of the primary proton beam was measured via its time of flight over the 10 metre distance across the experimental room. Two screens covered with material containing carbon could be moved into the path of the beam. One was located near the beam's entrance to the room and the other near the exit. A 2 X 2 inch plastic scintillator mounted on an RCA 8575 photomultiplier tube was used to detect the 4.43 MeV gamma rays emitted by the carbon on a screen while it was stopping the beam. A TAC was used to record the time of arrival of the gamma rays relative to a time reference obtained from the r.f. accelerating voltage on the cyclotron dees. The beam bursts were of sufficiently short duration that the centroids of the peaks in the resulting time spectra could be located with an accuracy of approximately 100 ps. It was arranged that the TAC received a stop pulse for every second reference pulse from the r.f. so that each spectrum contained two peaks. Their separation together with the r.f. frequency contributed sufficient information for a time scale calibration. Then, to determine the beam energy, it was only necessary to record a spectrum from each screen and to measure the lengths of the sides of the triangle whose apexes were the two screens and the scintillator. The accuracy of the determination is estimated to be 300 KeV at 50 MeV. This is comparable to the spread in the

beam energy in this beam line.

THE ONLINE COMPUTER

As previously mentioned, as many decisions as possible that were based on relationships between pulse heights were performed by the online computer because of the inherent flexibility it affords. The cross sections being measured were small enough for the count rates to be easily accomodated. The results of the online processing were used both to display the data in forms suitable for diagnostic purposes and to prevent the logging on magnetic tape of events that were clearly not of interest. Data was logged in unprocessed form in order to minimize the irreversable effects of any errors in the online processing.

For the purpose of display on a large CRT unit, data could be conditionally stored in memory in two forms, both of which represented the correlation between two parameters. These parameters could be chosen to be any of the words received by the computer from the ADC's. The first form was the usual two-dimensional array containing a frequency distribution of events. Two such arrays, each consisting of 64 X 64 9-bit words could be accommodated. The second form was a list of events, one to a word. In each half of a word was stored the value of one of the two parameters. All of the data in a list was displayed at once by cycling continuously through the list, illuminating one point for each event. The result is a scatter plot. Although a limited number of events may be included,

there are the significant advantages that each parameter is represented with relatively high (512 channel) resolution and a continuous range of event densities is depicted by the intensity of illumination or density of points. It followed that this was the form used during the preparation stage of each experimental run.

In the present measurements, the processing was relatively simple in that it consisted of only two types of determination. One was the testing of individual parameters in a manner similar to that employed by a single channel analyzer. The other was the testing for a particular correlation between pairs of parameters. A correlation was specified by drawing with the light pen on a display of the two parameters. Two lines were drawn as a function of either coordinate between which an event had to fall if this particular test were to yield a positive result. The first type of determination was used, for example, in the (p,2p) measurements to specify the time windows for reaction and chance coincidences. The second was used in all measurements to identify charged particles. In the case of a three detector telescope, two correlations were tested, epsilon versus sigma and delta versus sigma. Also, in the (p,pn) measurements, the neutron-gamma descrimination was performed by testing the correlation of PSD TAC output versus scintillator pulse height. The storage of events for display and the logging of events on tape could, independently of one another, be made contingent on any combination of the determinations being made. Periodically within the logging file

were placed the current values of the real-time clock and the accumulated charge in the Faraday cup corrected for computer and ADC dead time. This was in order that portions of a file could be analyzed seperately if the need arose.

DATA REDUCTION

Data reduction consisted primarily of the projection of the counts in each kinematic locus into a one-dimensional histogram whose abscissa represented the energy of the proton in the final state. Also, corrections for chance coincidences and pileups were applied and cross sections were computed from the projections.

The processing facilities employed during data reducion included those available during data acquisition together with considerably more generality concerning classification of events and their resultant destinations. Data could be displayed in the manners already described. However, an additional facility was used in connection with the storage of events in two display lists. Usually chance coincidence events were stored in one list and reaction events in the other. It was possible to effectively subtract the contents of the first list from the second while they were being accumulated. Whenever an event was scheduled to be stored in one of the lists, the other was searched for the event lying closest to it in the display area. If the separation was less than a specified amount, the events were cancelled. In this manner, all of the data for a particular pair of detector angles could

be stored and displayed together with high resolution, an achievement otherwise impossible with the available storage. Using a display from which chance coincidences had been subtracted, it was possible to more accurately specify with the light pen which events were to be included in the projection of the three body kinematic locus onto one proton energy axis. The data was ultimately expressed as a triple differential cross section $\frac{d^3\sigma}{d\Omega_1 d\Omega_2 dE_p}$ which was related to these projections by a multiplicative factor involving target thickness, beam flux, pileup rates, detector solid angles, neutron detector efficiency and the proton detector energy calibration.

EXPERIMENTAL UNCERTAINTIES

The most important contribution to uncertainties in the absolute magnitude of the cross sections is that involving target thickness. These are estimated to be as follows: ^{6}Li - 20%, ^{13}C - 10%, ^{12}C - 5%, ^{9}Be - 5%. For the (p,pn) measurements, there is the additional uncertainty associated with the calculation of the efficiency of the neutron detector. This is estimated to be 5%. Finally, the respective contributions from the beam flux measurement, solid angle measurements, counting losses and the proton energy calibration are estimated to be 2%,2%,3% and 2%. If these are added in quadrature, the overall uncertainties in the cross section magnitudes for the various reactions are as follows: ^{6}Li(p,2p) - 21%, ^{6}Li(p,pn) - 22%, ^{13}C(p,pn) - 13%, ^{9}Be(p,pn) and ^{12}C(p,pn) - 10%. Some indication of the reproducibility of the

measurements was derived by means of a comparison of $^{9}Be(p,pn)$ data acquired at the same angle pair during two different experimental runs. There were several differences in the experimental arrangements for these runs. In one case, only one neutron detector was used and a NaI(Tl) scintillator was used in place of a Si(Li) detector for the "E" counter. The difference in the resultant cross sections was marginally statistically significant.

3. EXPERIMENTAL RESULTS AND PWIA ANALYSIS

Five reactions were studied. These were $^{6}Li(p,2p)^{5}He$, $^{6}Li(p,pn)^{5}Li$, $^{9}Be(p,pn)^{8}Be$, $^{13}C(p,pn)^{12}C$ and $^{12}C(p,pn)^{11}C$. For each of the first four reactions, the number of angle pairs at which an energy correlation spectrum was acquired ranged from 6 to 10, most of which were quasi-free and the rest symmetric. $^{12}C(p,pn)$ was studied at only one angle pair because of its small cross section.

SCATTER PLOTS

An overview of the quality of data obtained for the various reactions is presented in the form of a number of typical scatter plots in figures 3.1 through 3.9. In the case of the (p,2p) reaction, the coordinates are the energies of the two final state protons while for (p,pn), the ordinate represents neutron time of flight with the scale reversed so that neutron energy increases in the upward direction. Chance coincidences have been subtracted by the technique described in the preceeding section. No correction for the variation of neutron detector efficiency with neutron energy has been applied at this point. Only events in the vicinity of significantly visible loci were recorded in order to ensure that there would be sufficient computer storage for these events.

In all cases the dominant three-body kinematic locus

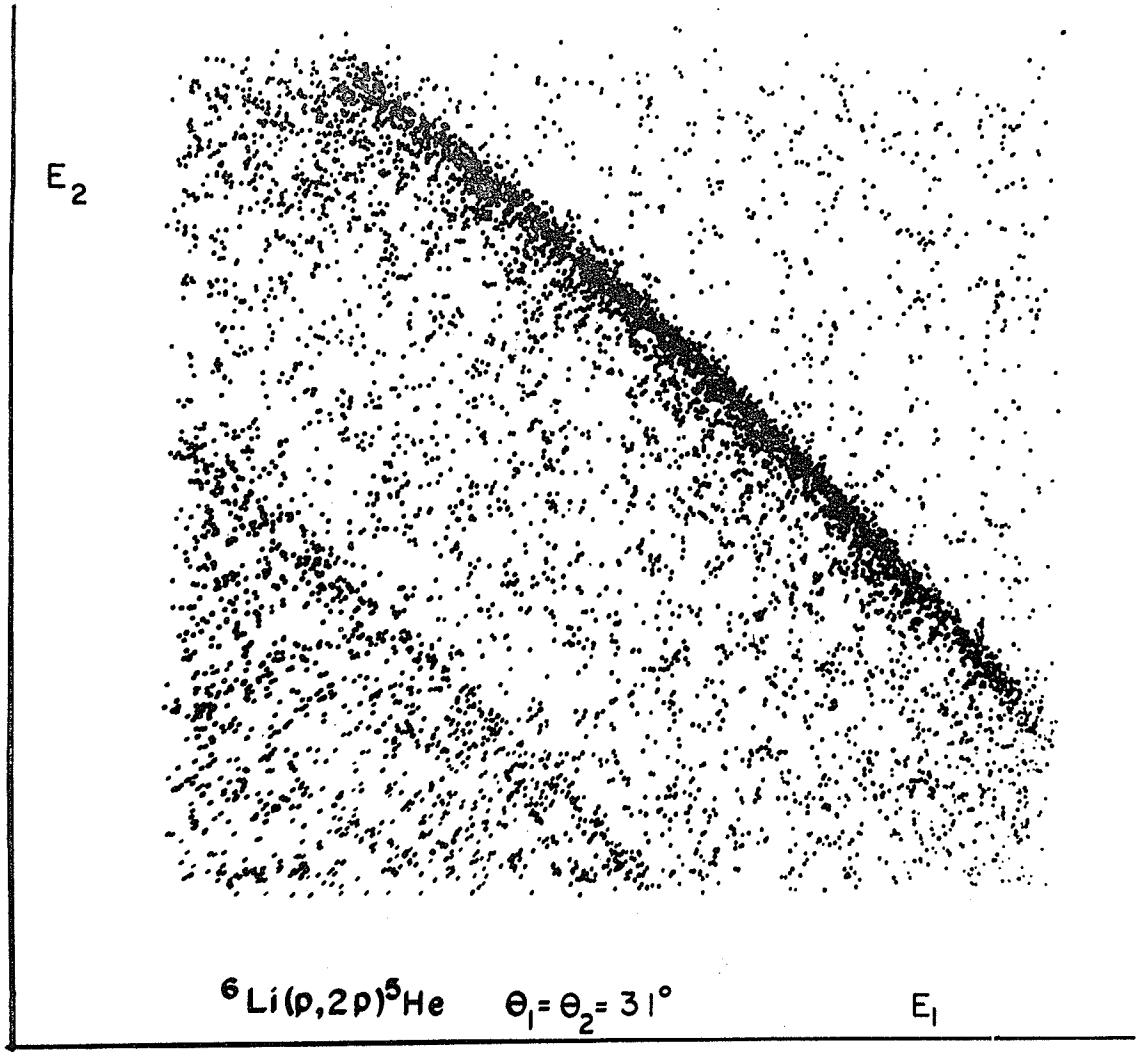

Fig. 3.1 Scatter plot for $^{6}Li(p,2p)^{5}He$ at 46 MeV with $\theta_1=\theta_2=31^{\circ}$.

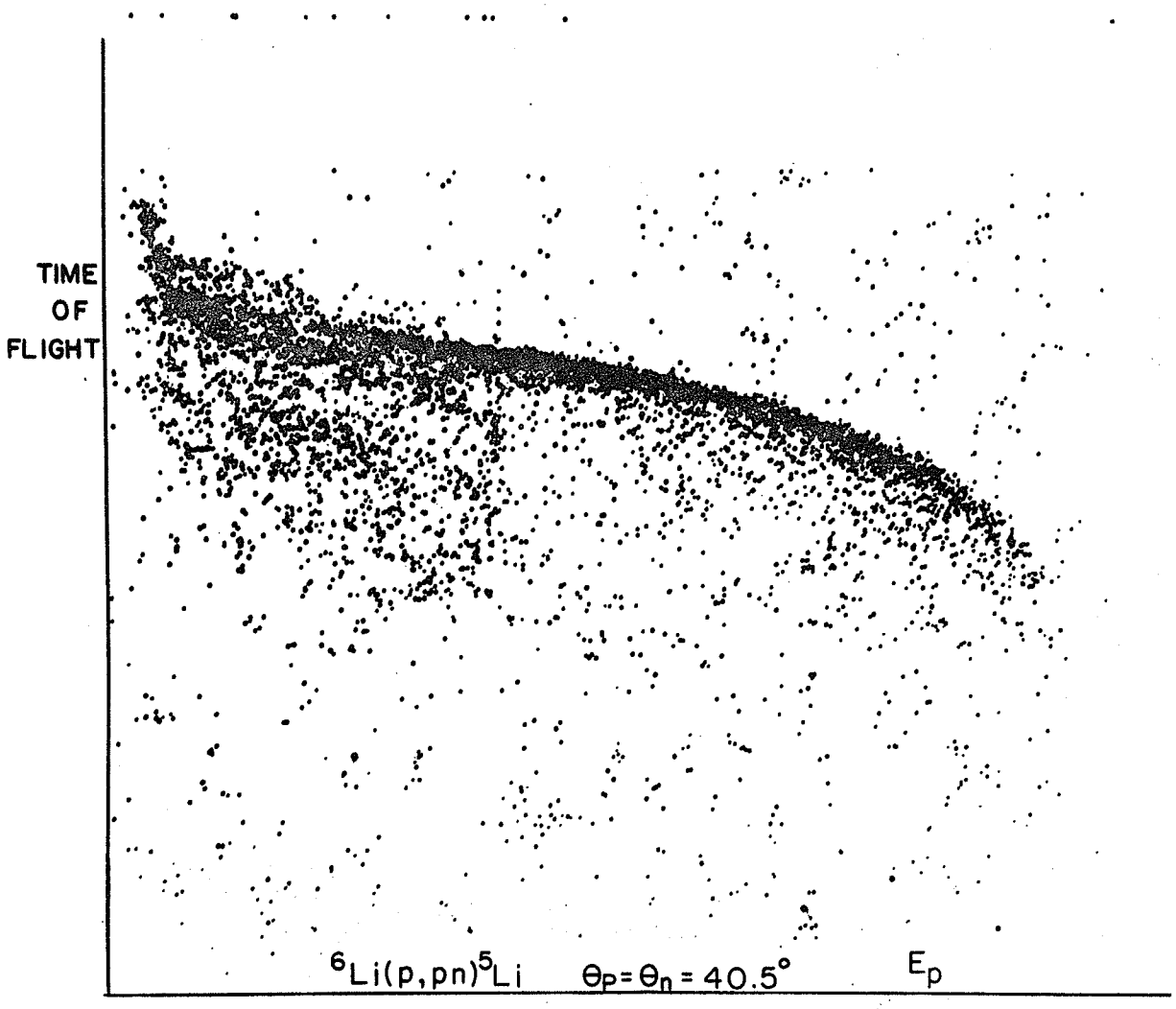

Fig. **3.2** Scatter plot for $^6Li(p,pn)^5Li$ at 46 MeV with $\theta_n=\theta_p=40.5°$.

Figures 3.3 through 3.5 Scatter plots for $^{9}Be(p,pn)^{8}Be$ at 45.7 MeV. The detector angles are shown on each figure.

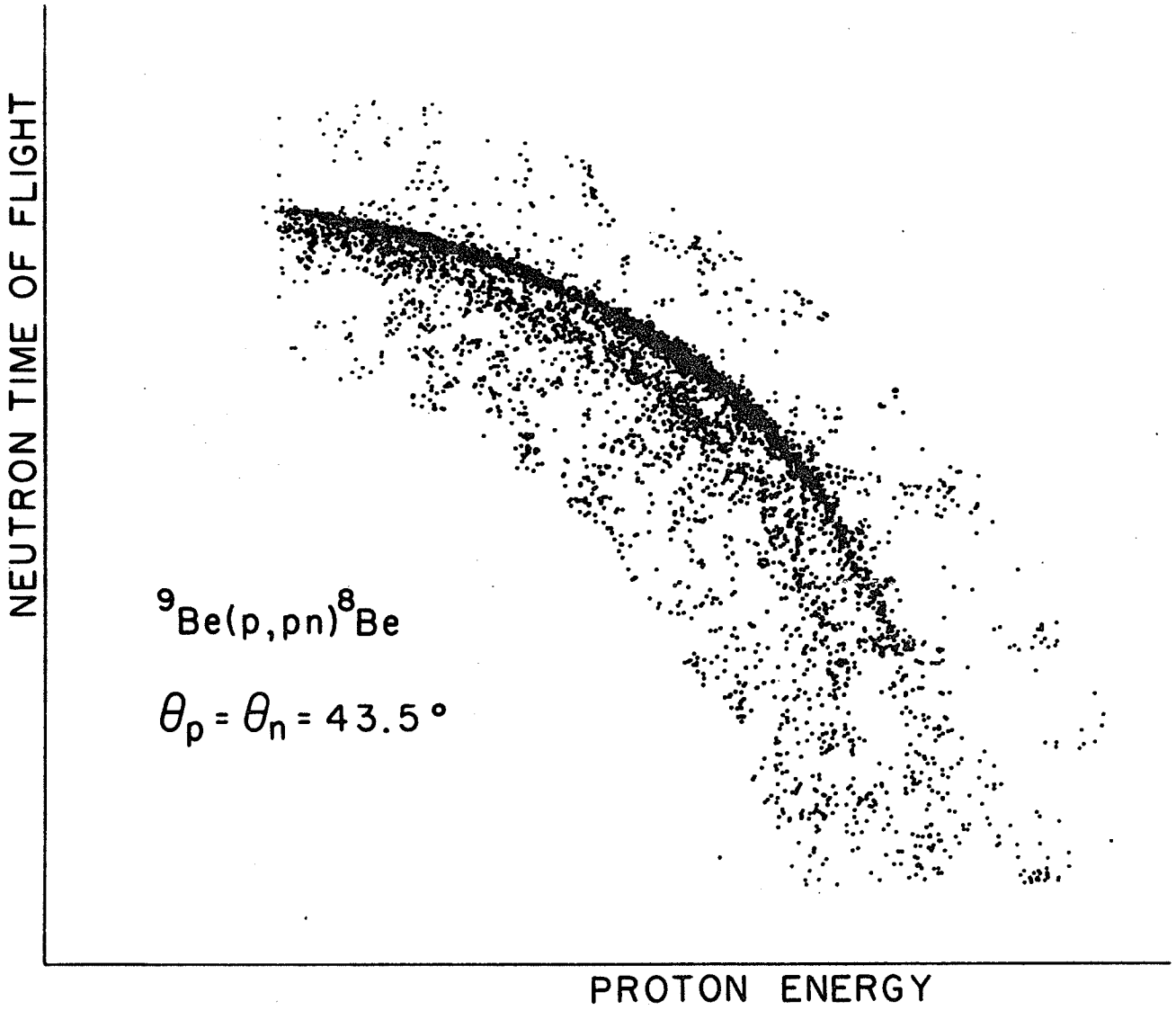
NEUTRON TIME OF FLIGHT
$^{9}Be(p,pn)^{8}Be$
$\theta_p = \theta_n = 43.5°$
PROTON ENERGY

Fig. 3.3

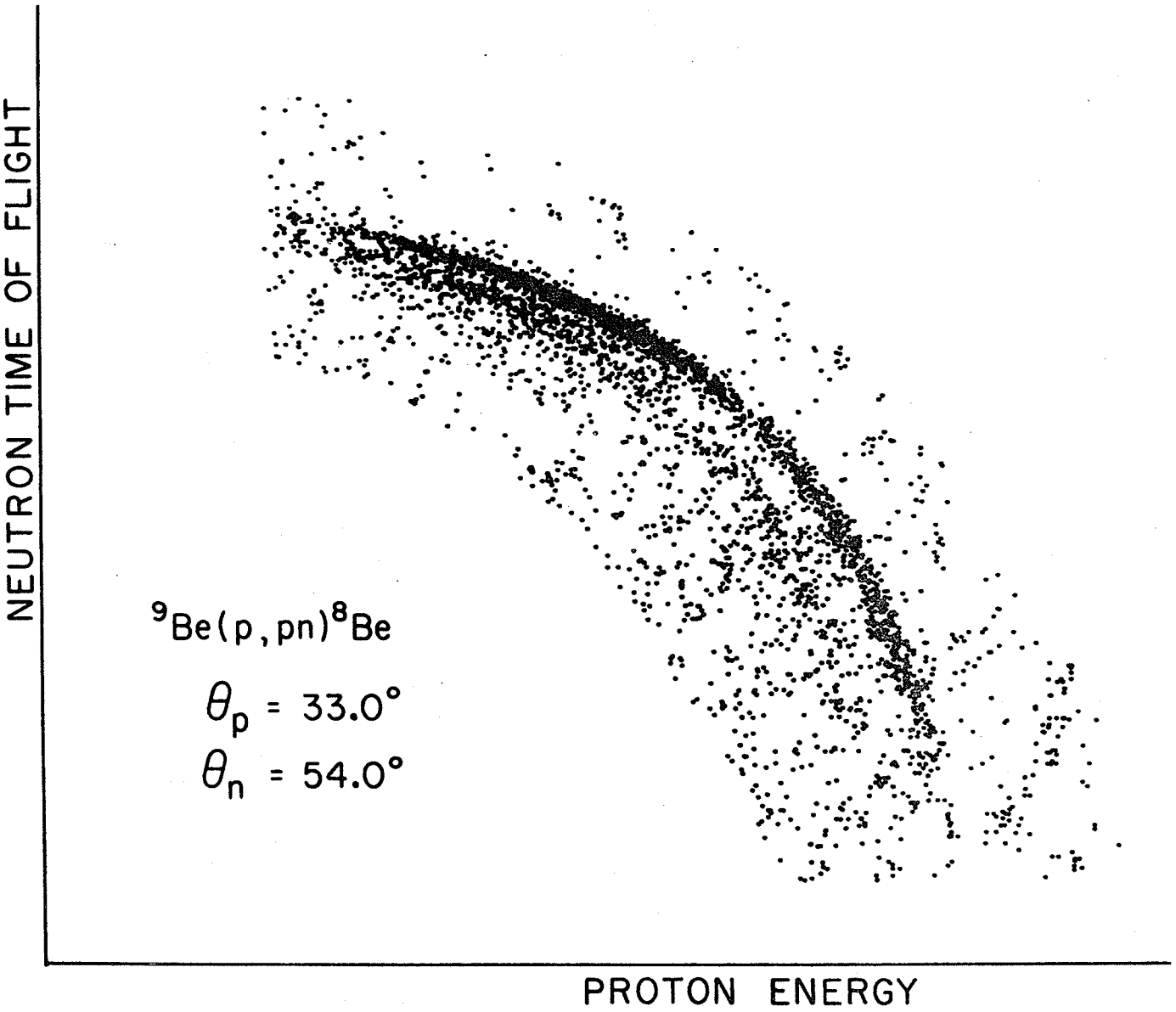
NEUTRON TIME OF FLIGHT
$^{9}Be(p,pn)^{8}Be$
θ_p = 33.0°
θ_n = 54.0°
PROTON ENERGY

Fig. 3.4

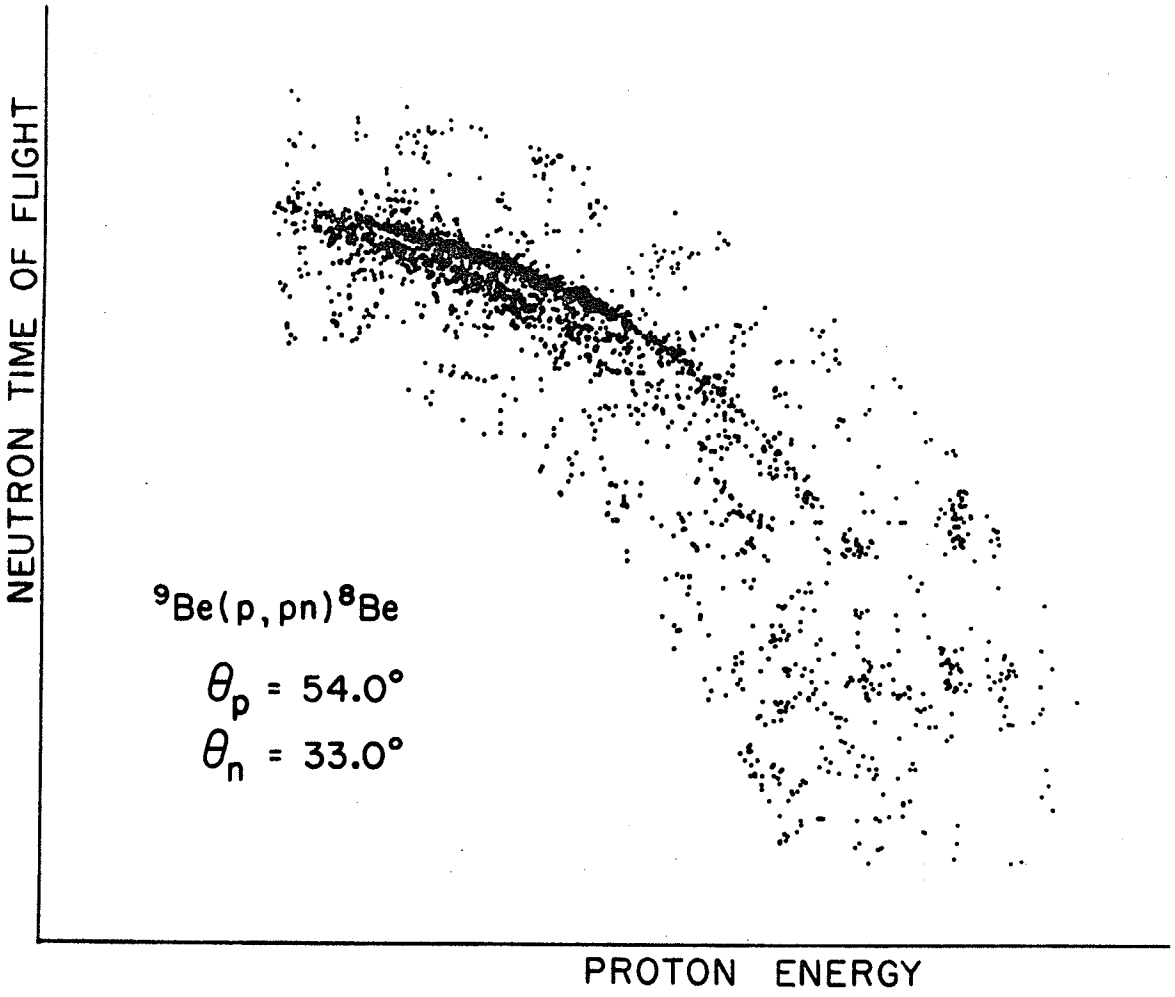
NEUTRON TIME OF FLIGHT
$^{9}Be(p,pn)^{8}Be$
θ_p = 54.0°
θ_n = 33.0°
PROTON ENERGY

Fig. 3.5

Figures 3.6 through 3.8 Scatter plots for $^{13}C(p,pn)^{12}C$ at 45.6 MeV. The detector angles are shown on each figure.

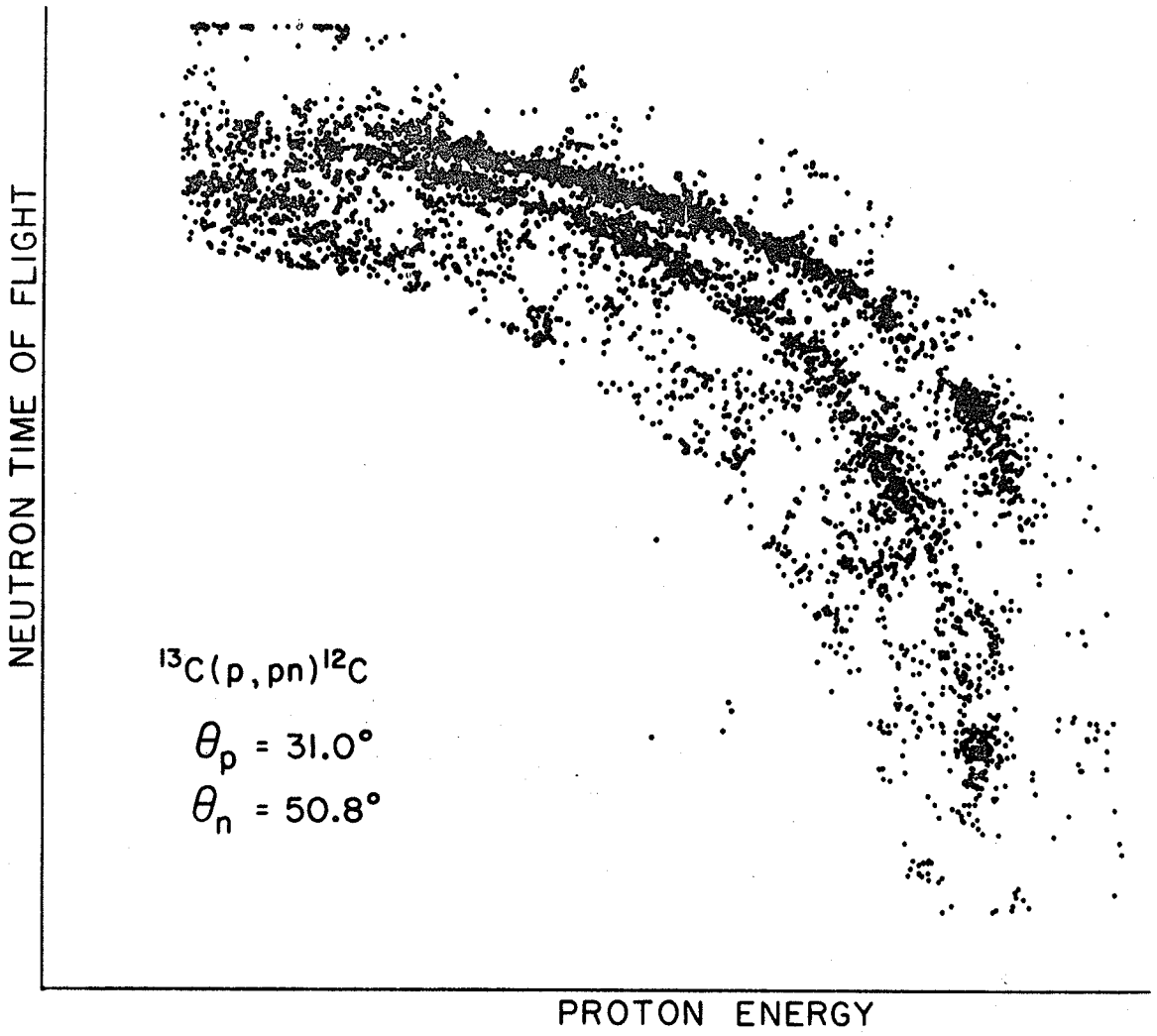
NEUTRON TIME OF FLIGHT
PROTON ENERGY
$^{13}C(p,pn)^{12}C$
θ_p = 31.0°
θ_n = 50.8°

Fig. 3.6

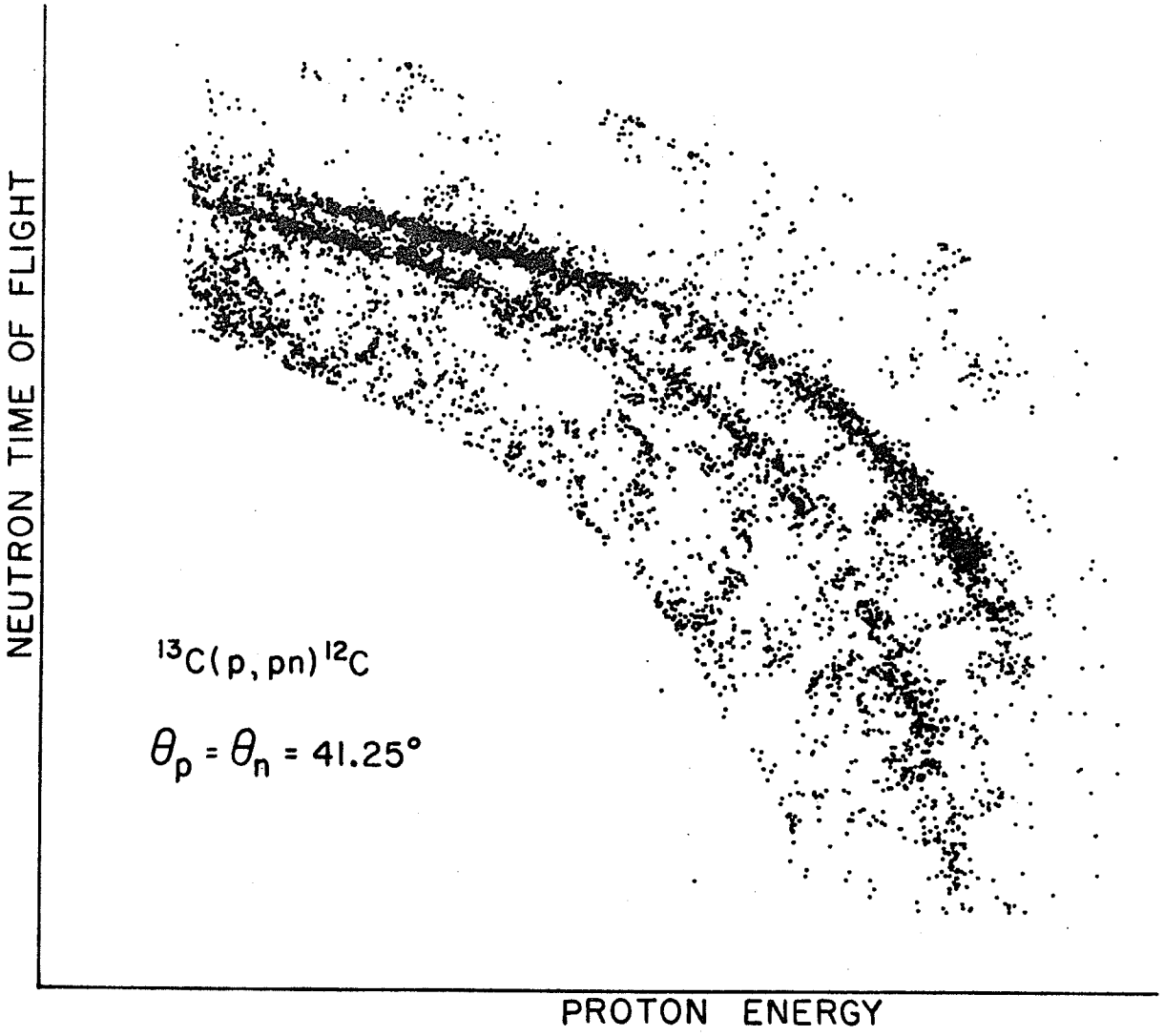
NEUTRON TIME OF FLIGHT
$^{13}C(p, pn)^{12}C$
$\theta_p = \theta_n = 41.25°$
PROTON ENERGY

Fig. 3.7

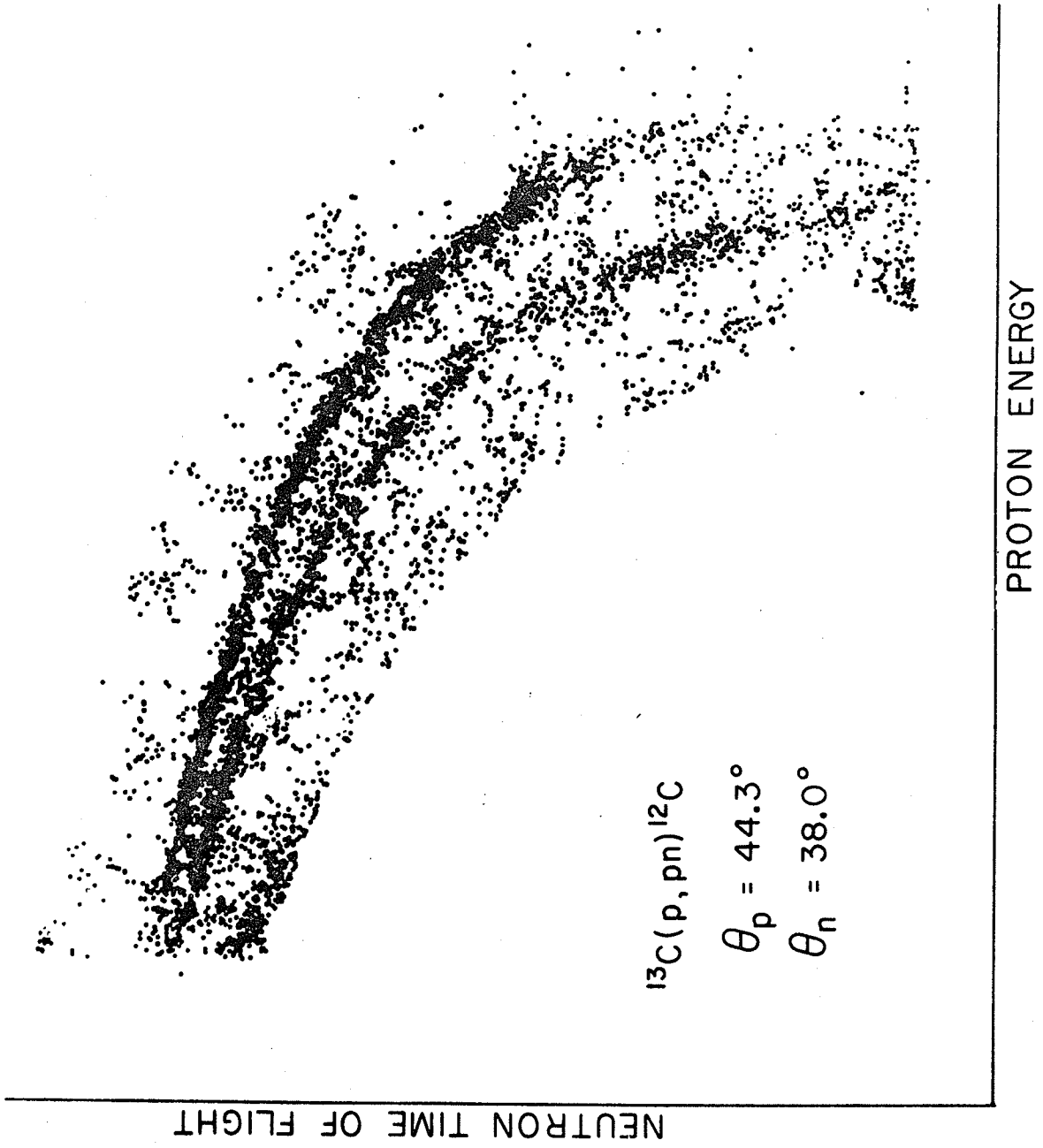
NEUTRON TIME OF FLIGHT
PROTON ENERGY
$^{13}C(p,pn)^{12}C$
$\theta_p = 44.3°$
$\theta_n = 38.0°$

Fig. 3.8

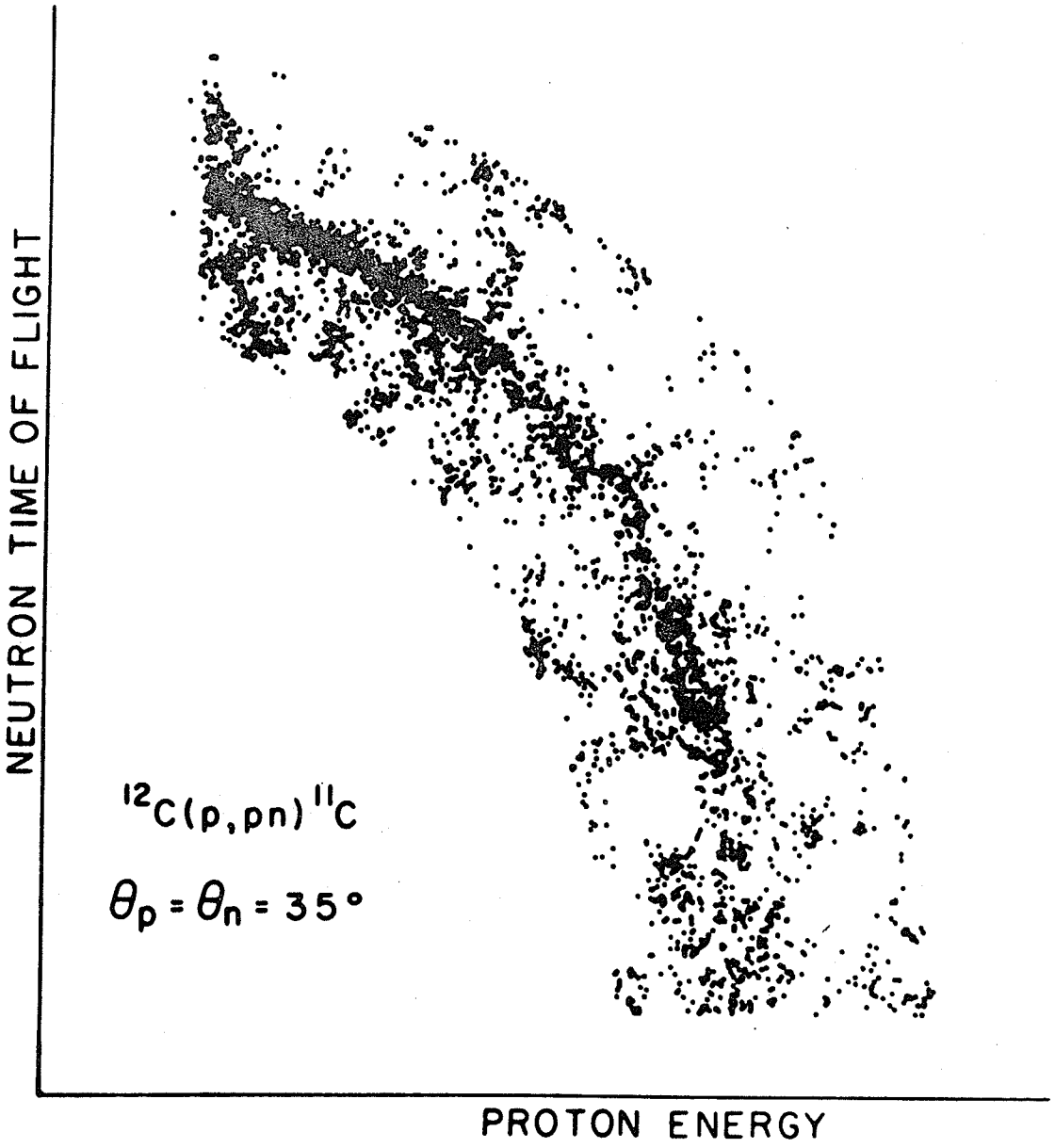

Fig. 3.9 Scatter plot for $^{12}C(p,pn)^{11}C$ at 45.6 MeV

corresponds to the transition to the ground state of the residual nucleus. As well, the loci corresponding to the first excited state of ^{8}Be (2.9 MeV) and ^{12}C (4.43 MeV) are clearly visible in the respective ^{9}Be and ^{13}C data. The length of the neutron flight path was chosen to be just long enough to provide sufficient resolution to clearly seperate the ^{8}Be state from the ground state. Because the state in ^{12}C is so high in excitation, the corresponding flight path could be reduced to the minimum defined by the largest acceptable detector solid angle. There is a faintly-visible locus near the origin of the ^{6}Li(p,2p) plot, the Q-value of which corresponds to the excitation of the 16.7 MeV 3/2^{+} state in ^{5}He. The very small population of this state at this energy is consistent with the marked trend established by all the higher energy ^{6}Li(p,2p) data (M72,R67,T66). As the bombarding energy decreases, the ratio of the cross section of the 16.7 MeV state to that of the ground state also decreases. For example, at 100 MeV, this ratio is approximately .5 while at 460 MeV it is larger than unity.

Since the proton detector telescope used for the ^{6}Li(p,pn) measurements included no epsilon detector, charged particle identification was not possible below 10.5 MeV. For this reason, there are visible in this region of the scatter plot considerable background from other reactions. Consequently, data from this region was not included in the projections to be shown later. The upward bend of the leftmost end of the ^{6}Li(p,pn) locus is due to timing walk of the constant fraction

discriminator for the proton signal.

For the reactions on ^{6}Li, the residual nuclei ^{5}He and ^{5}Li are unbound by 0.96 MeV and 1.96 MeV with widths of .58 MeV and approximately 1.5 MeV, respectively. Although the corresponding loci are visibly wider than those for the other reactions, they still have the distinctive appearance associated with a three-body final state. However, this unbound nature of the residual will be later seen to have other important ramifications.

Careful examination of the central region of the ground state loci of the ^{9}Be and ^{13}C scatter plots reveals that there is a narrow area on each of them with a much lower event density. These are the points at which the recoil momentum is near zero. The Plane Wave Impulse Approximation (PWIA) predicts that knock-out of a p-state nucleon will result in a minimum cross section under such conditions.

Finally, on the ^{13}C loci, there are visible relatively small areas where the event rate is strongly enhanced. These are attributed to sequential processes which presumably are either

$$^{13}C(p,p')^{13}C^{+}$$
$$\hookrightarrow {}^{12}C + n$$

or $$^{13}C(p,n)^{13}N^{+}$$
$$\hookrightarrow {}^{12}C + p$$

In either case, the excitation of the intermediate state is so high that there many possibilities for its identity. These processes will be more clearly visible as peaks in the

projections of the data.

Q-VALUE SPECTRA

Some of the data is presented in another form in figures 3.10 through 3.12. These show histograms obtained by projecting onto an abscissa proportional to the Q-value of the reaction those events for which the energy of the two final state nucleons differ by less than a specified amount. In this way, the relative excitation of the states of the residual nucleus is more clearly illustrated. It should be born in mind that the result may be distorted by the neutron detector efficiency variation but this effect should be small for ranges in excitation energy of a few MeV. It is of interest to compare these spectra with those obtained from the (p,d) reaction on the same targets since the spectroscopic factors should be the same in both cases. Such a comparison of $^{12}C(p,2p)$ and $^{12}C(p,d)$ was made by Pugh et al (P65) on the assumption that the structure of ^{12}C would be similar with respect to protons and neutrons. As can be seen from their result which is reproduced in the upper part of figure 3.10, there is good agreement at the angles chosen for the comparison. The present data for (p,pn) is shown below theirs. It has poorer resolution but it is consistent with the other reactions.

This is in sharp contrast with the comparisons of (p,d) and (p,pn) on ^{13}C and ^{9}Be. For (p,d) on both targets (T68,V67), the first excited state is more strongly populated than the ground state while for (p,pn), the reverse is true. In the case

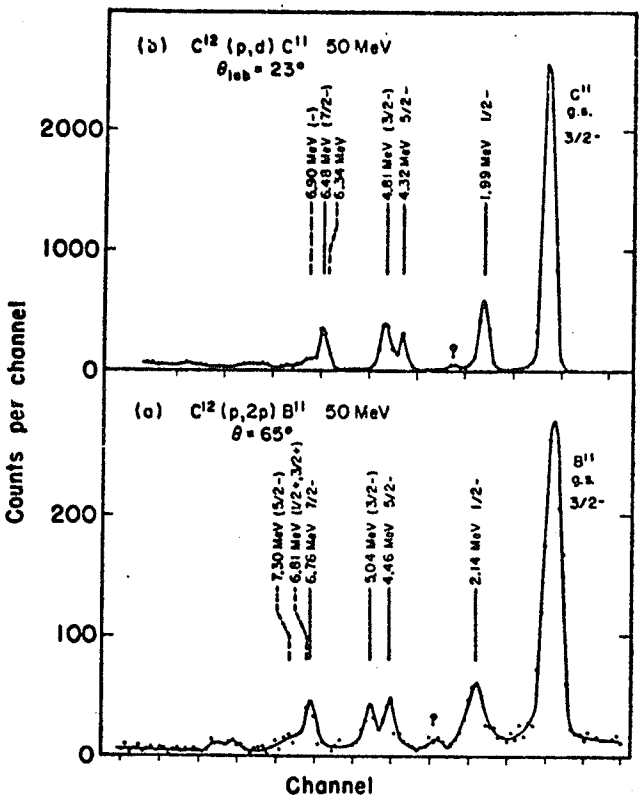

(a) A summed energy spectrum (E_1+E_2) for the reaction $C^{12}(p,2p)B^{11}$ at 50 MeV. The positions of known excited states of B^{11} are indicated. (b) A deuteron energy spectrum from the reaction $C^{12}(p,d)C^{11}$ at 50 MeV. The positions of known excited states of C^{11} are indicated.

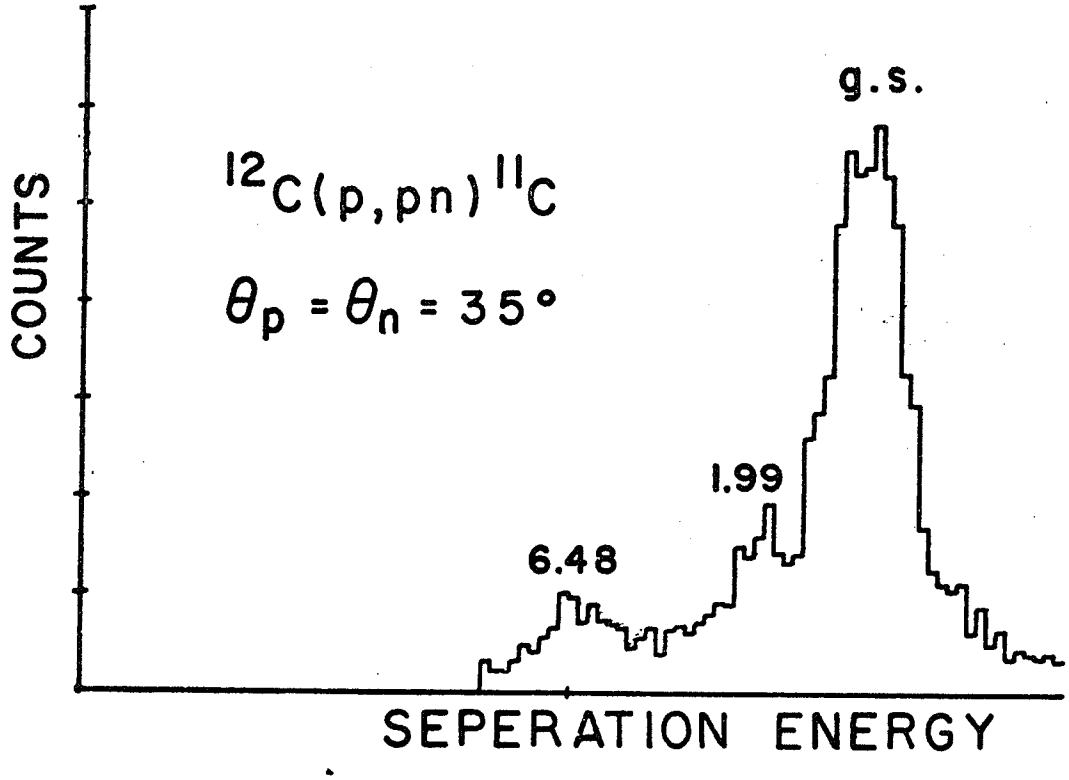

Fig. 3.10 Reproduction of a figure from (P65) together with a Q-value spectrum for $^{12}C(p,pn)^{11}C$ at 45.6 MeV.

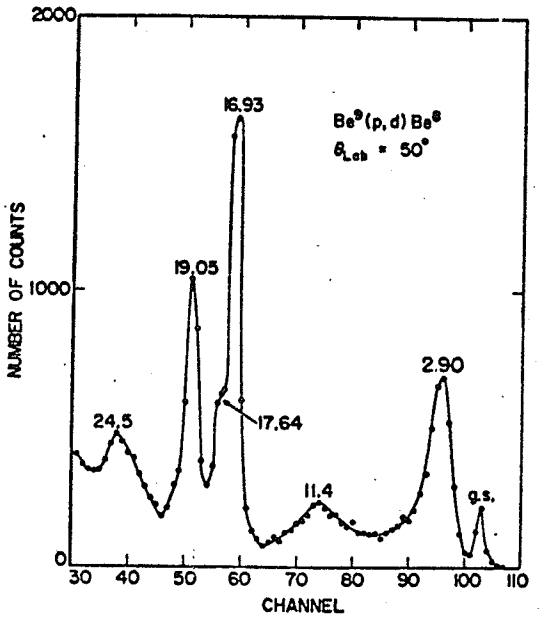

Deuteron spectrum for $\theta_{Lab} = 50°$ from the reaction $Be^9(p,d)Be^8$.

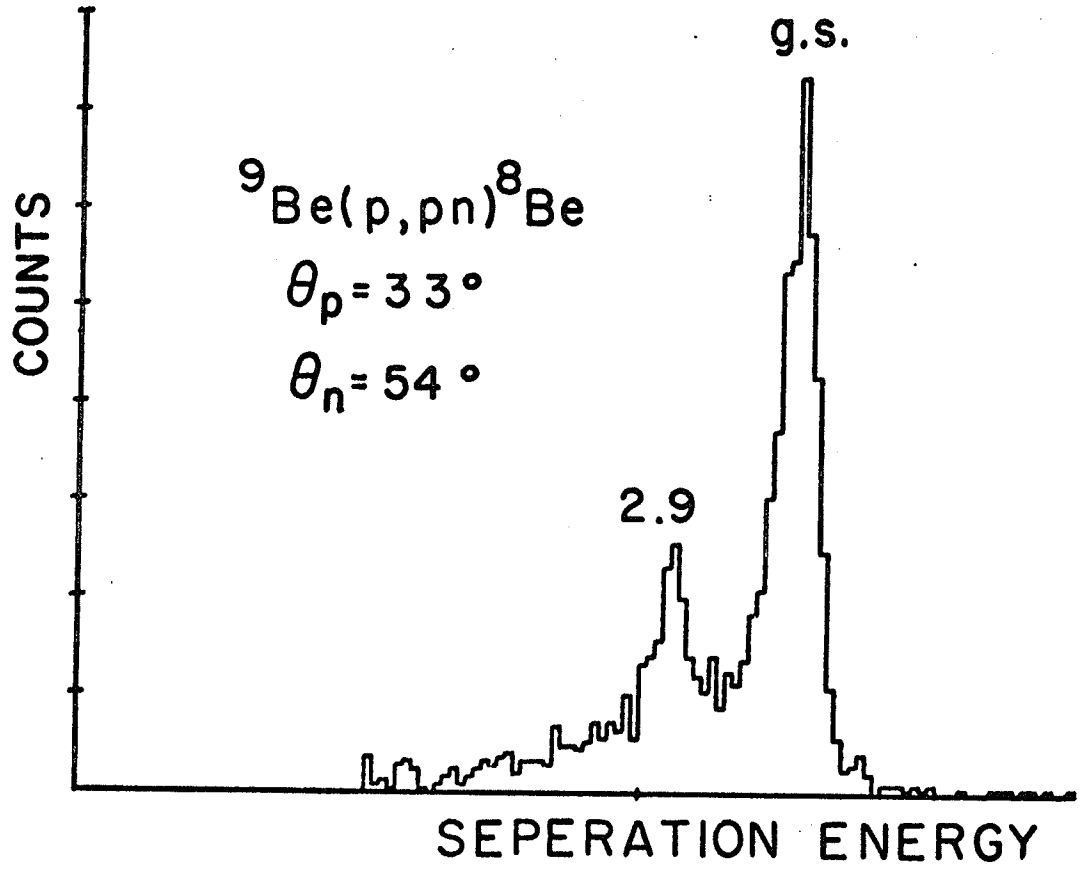

Fig. 3.11 Reproduction of a figure from (V67) together with a Q-value spectrum for $^9Be(p,pn)^8Be$ at 45.7 MeV.

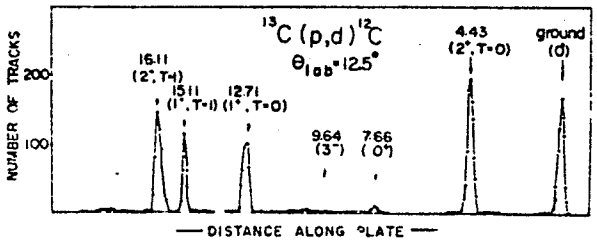

Deuteron spectrum from the reaction $^{13}C(p,d)^{12}C$. Two peaks, corresponding to the two lowest-energy states from the $^{12}C(p,d)^{11}C$ reaction, are omitted.

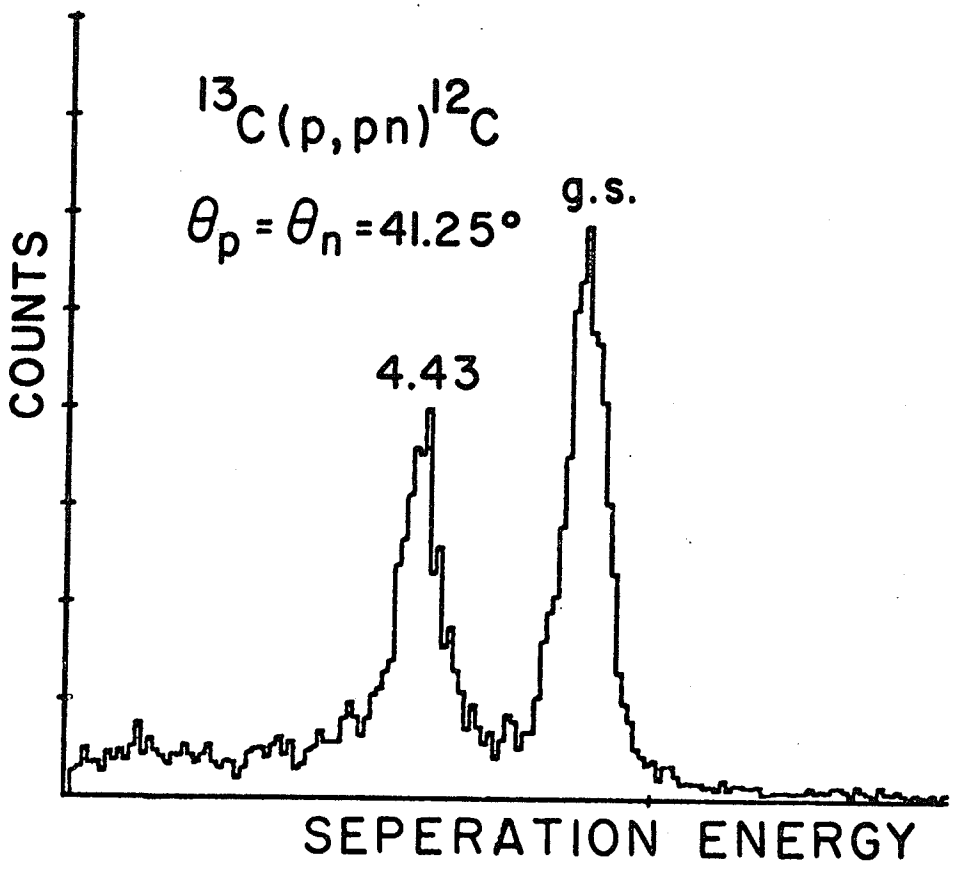

Fig. 3.12 Reproduction of a figure from (T68) together with a Q-value spectrum for $^{13}C(p,pn)^{12}C$ at 45.7 MeV.

of ^{9}Be, this difference is especially dramatic. A comparison of the angular distributions of the (p,d) reactions verifies that the relative dominance of the excited states is not specific to the particular angles chosen for the comparison with (p,pn).

An observation that may shed some light on these differences is that the kinematic conditions of the (p,d) and (p,pn) reactions cause them to be sensitive to different parts of the initial bound state wave function of the ejected neutron. The (p,pn) reaction probes the low momentum components while the (p,d) reaction emphasizes the high momentum components. In the binding energy formalism, the initial bound state is represented as the neutron bound to the final state of the residual nucleus. If this final state is excited, the binding energy is correspondingly larger to conserve energy. In the cases of ^{9}Be and ^{13}C, this represents a substantial percentage difference in binding energy so that the wave functions bound to the excited states are enhanced in the region of large momentum, yielding a larger cross section for (p,d) and smaller for (p,pn). The binding energy for the ^{12}C target is so large that the percentage increase for the excited state of ^{11}C is too small to have much effect.

PWIA ANALYSIS

The data will now be compared with the PWIA. This is not done for the purpose of obtaining a detailed fit yielding nuclear structure information. Rather it is done in the hope

that the nature of the discrepancies between the PWIA and the data will give some information about the reaction mechanism complexities contributing to these discrepancies.

Eqn. 1.1 gives the expression for the cross section in the PWIA. For convenience it is reproduced here.

$$\frac{d^3\sigma}{d\Omega_1 d\Omega_2 dE_1} = PSF \quad \frac{d\sigma}{d\Omega}\Big)_{12} \quad |\phi(\underline{K})|^2 \qquad 1.1$$

The first factor, PSF, which contains kinematic and phase space effects is the same as that given in eqn. 4.18 for a different calculation. $\frac{d\sigma}{d\Omega}\Big)_{12}$ is the two nucleon differential scattering cross section evaluated in the centre of mass. As is pointed out in (J70), the fact that this cross section is being used to approximate an off-mass shell cross section means that there is an ambiguity concerning the choice of the energy and angle at which it is to be evaluated. At least four different prescriptions have been used in previous work. These are that the kinematic conditions are taken to be those in:

1) the centre of mass of the scattering nucleons in the final state,

2) the centre of mass of these nucleons in the initial state,

3) the laboratory frame, taking the ejected nucleon to be initially at rest, or

4) that the kinematic conditions are taken to be those yielding the same momentum transfer from the incident particle. It has been found that for other reactions such as $^6Li(\alpha, 2\alpha)d$, prescription 1 seems most consistent with the data

(W71,P69,G70). Consequently, it was adopted here. For the present reactions, the choice can be expected to influence only the absolute magnitude of the result since the nucleon-nucleon cross section varies monotonically with energy and is fairly isotropic.

In the interests of convenience, $\phi(K)$ was computed as the Fourier transform of analytic spatial wave functions of the form used by Tyren et al (T66) for the analysis of their 460 MeV (p,2p) data. The unnormalized radial function is given by

$$R_\ell(r) = f_\ell(\alpha r)\ h_\ell^{(1)}(i\alpha r)$$

where $h_\ell^{(1)}$ is the spherical Hankel function of the first kind which ensures that the wave function has the correct asymptotic behavior for the known binding energy.

$$\alpha = \frac{\sqrt{2\mu\epsilon}}{\hbar}$$

where μ is the reduced mass of the ejected nucleon and ϵ is the binding energy.

$$f_\ell(\rho) = \left[3 - 4e^{-\beta\rho} + e^{-2\beta\rho}\right]^{2\ell+1} \left[1 + \delta_{\ell,0}\left(\frac{1-e^{-\gamma\rho}}{\gamma}\right) + a_2\left(\frac{1-e^{-\gamma\rho}}{\gamma}\right)^2\right]$$

where β, γ and a_2 are parameters controlling the shape of the corresponding potential. Tyren et al imply that their practice of choosing $\beta = \gamma$ results in an approximately flat-bottomed potential well with a rather large diffuseness. This was adopted in the present calculations. For ^{6}Li, the parameters were taken to be the same as those used by Tyren et al while for ^{9}Be and ^{13}C, they were adjusted to obtain the optimum fit

to the shapes of the projections of the energy correlation spectra while arbitrarily normalizing the theory to the data at each angle pair. It was empirically found that the value of a_2 was much less important than that of β (=γ). This is probably because β and γ influence the RMS radius of the wave function much more than a_2 and the RMS radius is the only important property in the present context. The parameter values and corresponding RMS radii yielding the best fits are listed in table 3.1.

Figures 3.13 through 3.15 show the projections of some of the data compared with the results of the calculations. The error bars represent statistical uncertainties only. All of the available data for the (p,2p) and (p,pn) reactions on ^{6}Li are shown in figures 3.13 and 3.14, respectively. Two different bombarding energies are included for ^{6}Li(p,2p). If the spectra in these figures are viewed in a sequence moving down the first column and then down the second, the quasi-free angle pairs appear first and in order of increasing proton angle. Such angle pairs can be recognized by the fact that the PWIA goes to zero at zero recoil momentum. Following the quasi-free angles are some symmetric angles both more forward and backward than the quasi-free symmetric angles. Then, in figure 3.15, all of the quasi-free angle pairs for both ^{9}Be and ^{13}C are shown together with those for ^{6}Li(p,pn) for convenient comparison. All of these reactions were studied at approximately 46 MeV. It can be seen that for ^{9}Be, the shapes of the spectra are quite similar to those predicted by the PWIA although the independent

TABLE 3.1

Parameters for the p-shell wavefunctions used in the calculated cross section in figure 1. The r.m.s. radii are also tabulated.

Reaction	E_s(MeV)	$\beta=\gamma$	a_2	$\sqrt{\langle r^2 \rangle}$
$^{6}Li(p,2p)^{5}He$ (a)	4.655	.740	.736	5.310
$^{6}Li(p,pn)^{5}Li$	5.622	.740	.736	4.810
$^{9}Be(p,pn)^{8}Be$	1.665	1.200	.700	6.599
$^{13}C(p,pn)^{12}C$	4.947	.500	.700	5.935

(a) Same as for 460 MeV

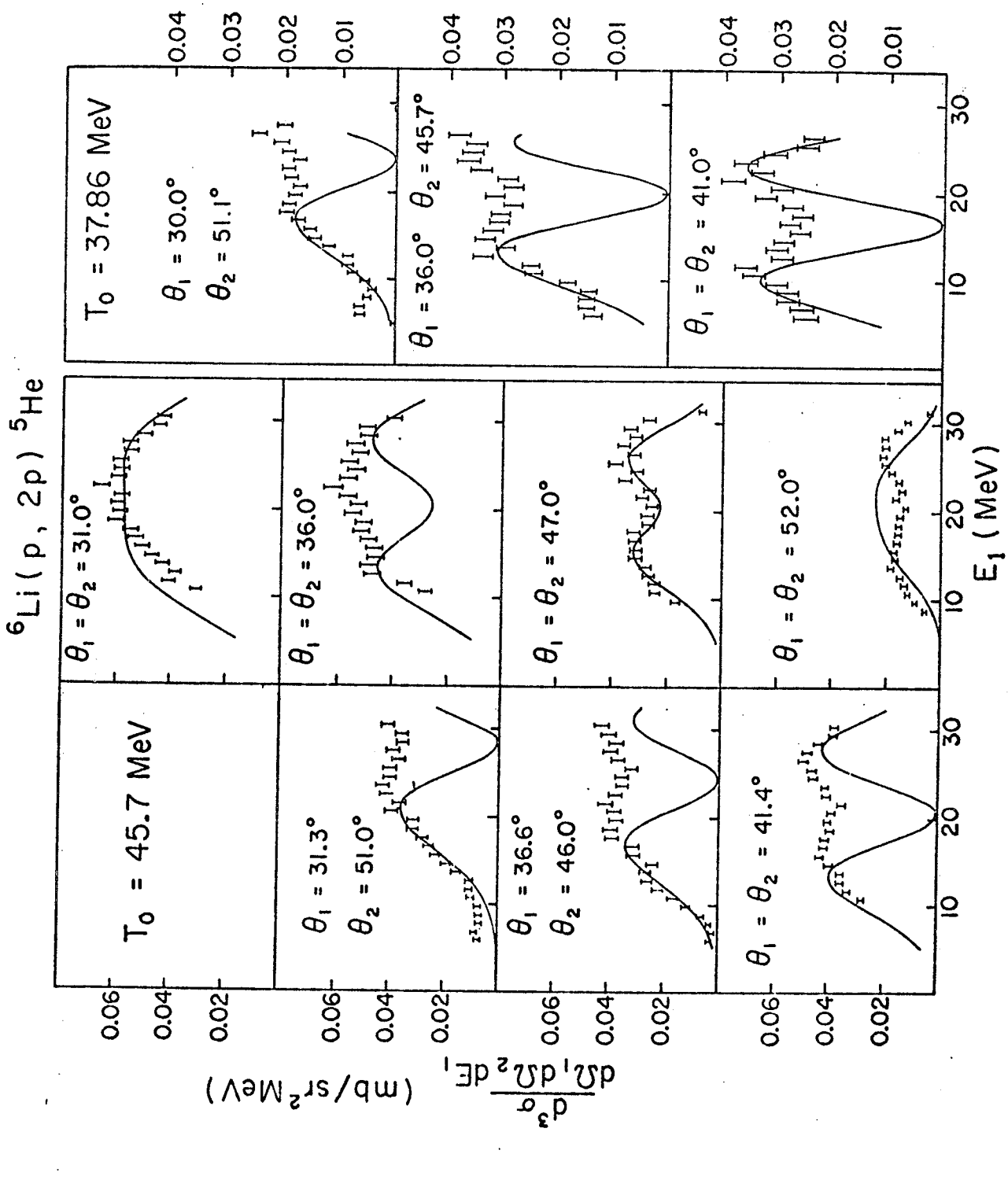

Fig. 3.13 The cross sections for ^{6}Li(p,2p)^{5}He at 45.7 and 37.86 MeV compared with the arbitrarily normalized PWIA calculations.

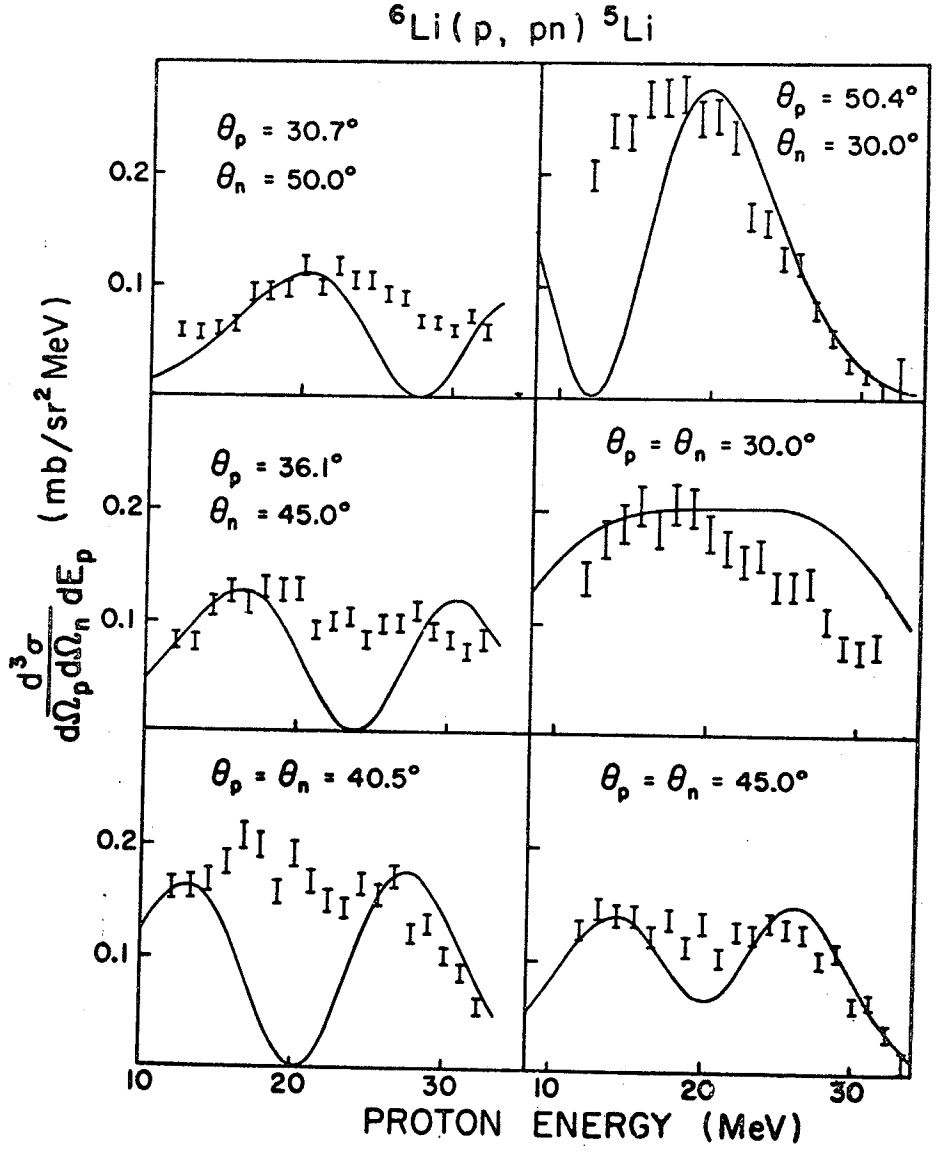

Fig. 3.14 The cross sections for ^{6}Li(p,pn)^{5}Li at 46.1 MeV compared with the arbitrarily normalized PWIA calculations.

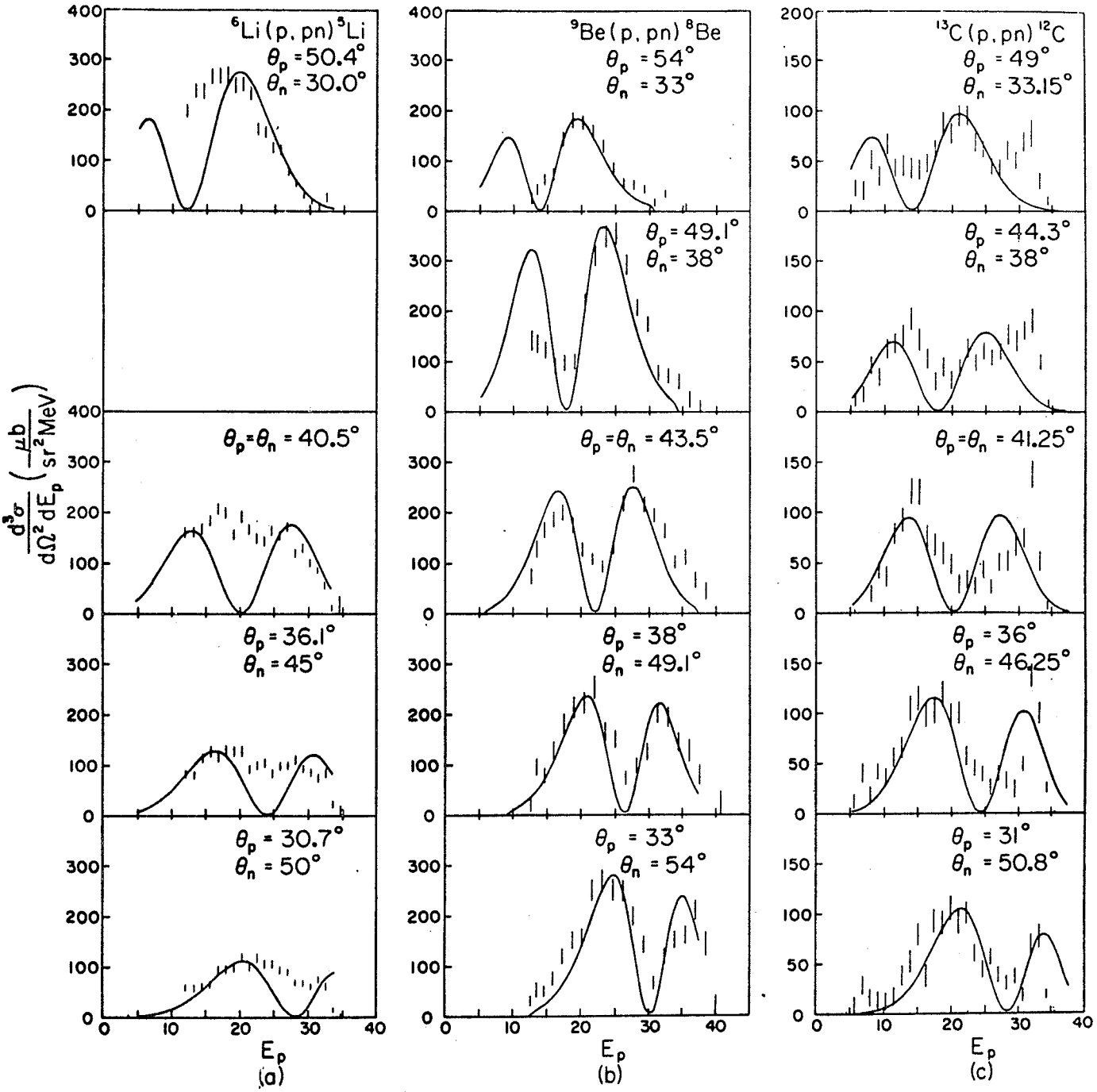

Fig. 3.15 The cross sections at quasi-free angles for the three (p,pn) reactions indicated. The solid curves are the arbitrarily normalized results of the PWIA calculations.

normalization at each angle pair should be born in mind. The PWIA would predict an essentially isotropic angular behavior while the data shows significant variation. For ^{13}C, there is also a similarity between the data and the curves but the comparison is made more difficult by the poorer statistical accuracy of the data because of the much lower cross section and by the presence of the sequential processes. These are recognizable as a strong peak (or peaks) at approximately 12 MeV and a weaker one at 14 MeV.

For both ^{9}Be and ^{13}C, the data exhibits the deep p-state minima predicted by the PWIA. This is not the case with $^{6}Li(p,2p)$ or (p,pn). With these reactions, the tails of the recoil momentum distributions are fitted fairly well but the minima in the data at zero momentum are very shallow. This is consistent with the results of recent studies of the $^{6}Li(p,2p)$ reaction at higher energies of 100 and 156 MeV where, in both angular and energy correlations, minima were either not observed or were very shallow (M72,R67). Earlier measurements (T66) had been inclusive because their recoil momentum resolution was poor enough to have acounted for the effect. When this was pointed out, it was widely believed that this was the basis of the phenomenon (M68). It had been established that calculations including distorted waves could not reproduce any significant "filling in" of the angular correlation distribution.

It was then pointed out by Saito et al (S68) that the observed effects can be explained by taking into account the

(related) facts that the residual nucleus is unbound and that the ^{6}Li target nucleus is well described as an alpha-deuteron cluster structure. Their cluster wave function, which is consistent with the known properties of the ^{6}Li ground state including the charge form factor from electron scattering, consists of a deutron cluster in an internal 1s state bound to an alpha cluster in a relative 2S state. When such a wave function is transformed into the coordinates of the outer proton and neutron relative to the centre of total mass, it can be seen to have a substantial component with both of these nucleons in 2s states as well as the 1p states predicted by the simple shell model. (It should be noted that such a shell model cannot fit the charge distribution of ^{6}Li). Now the unbound residual nucleus, ^{5}He or ^{5}Li, contains not only the $p_{3/2}$ resonance but also the $s_{1/2}$ continuum so that a one-step knock-out process of one of the nucleons from the 2s component of ^{6}Li can conserve parity. The plane wave calculations of Saito et al, which include this possibility, are in qualitative agreement with the 155 MeV ^{6}Li(p,2p) data.

A comparison of the present measurements of the (p,2p) and (p,pn) cross sections yields further evidence of the importance of the deuteron cluster structure of ^{6}Li. An examination of the angular dependences of the cross sections at quasi-free angles reveals that, while those for (p,2p) are almost constant, the (p,pn) cross section rises monotonically by a factor of three as the proton angle increases. This is strongly reminiscent of the results of a similar comparison of these two reactions on

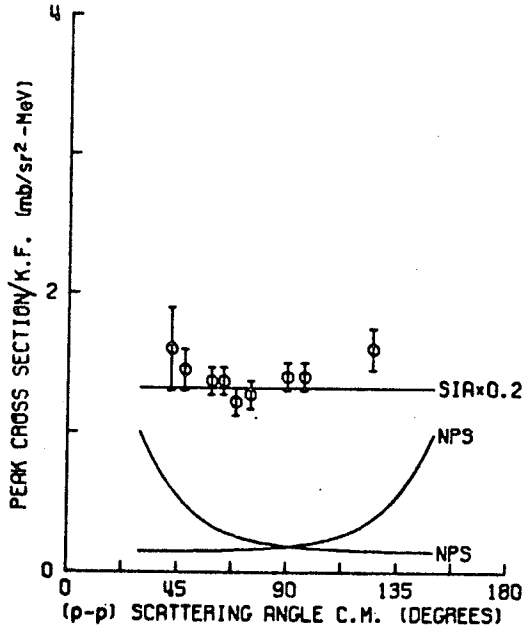

The angular distribution of p-p quasielastic scattering. The peak cross sections have been divided by the kinematic factor. The curves indicate the angular distributions expected from contributions from the SIA and from the two possible n-p singlet final-state interactions.

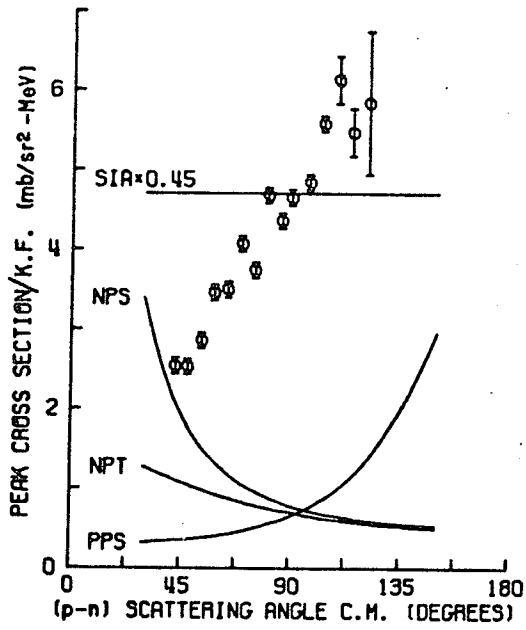

The angular distribution of p-n quasielastic scattering. The solid curves show the angular distributions expected from contributions from the SIA, the p-p singlet FSI, the n-p singlet FSI, and the n-p triplet FSI.

Fig. 3.16 Reproduction of a figure from (P71) showing the angular dependence of the D(p,2p)n and D(p,pn)p cross sections. SIA (Simple Impulse Approximation) is another designation for the PWIA of the present work and FSI refers to a theoretical calculation including the final state interaction of pairs of nucleons.

deuterium. Figure 3.16 shows a reproduction from Peterson et al (P71) of their experimental peak cross sections for these reactions plotted as a function of the two-nucleon scattering angle in their centre of mass. It should be noted that this angular variation of the (p,pn) cross section does not seem to be a general property of the reaction mechanism since there is no such monotonic variation in the results from ^{9}Be or ^{13}C. There is another analogy with the results from deuterium. Although only two different bombarding energies are available for ^{6}Li in this energy region, it can be stated that the cross sections for the (p,2p) reactions on both ^{6}Li and deuterium (M70) show a marked variation with incident energy. In both cases, the cross section rises by approximately 25% while the energy increases from 38 to 46 MeV. It is interesting to note that, at 100 MeV, the (p,2p) cross section (M72) is larger by approximately a factor of four so that it is comparable to the (p,pn) cross section at 46 MeV.

Another important difference between the (p,2p) and (p,pn) cross sections is that the average magnitude of the ^{6}Li(p,pn) cross section is approximately four times that for (p,2p) at the same bombarding energy of 46 MeV. A similar relationship has been observed for D(p,pn) and D(p,2p) although that ratio is only approximately 2.5 at this energy (P70,M70). The primary reason for undertaking the ^{12}C(p,pn) measurement was to resolve the uncertainty as to whether this unexpectedly large difference in the cross sections was associated with the structure of ^{6}Li or was a general property of the reaction

mechanisms. The very large neutron seperation energy of ^{12}C (18.72 MeV) exceeds the proton seperation energy by about 3 MeV and therefore should tend to suppress the (p,pn) cross section relative to (p,2p). The result of the measurement was that the (p,pn) cross section was found to be significantly larger than for (p,2p) but the difference is only as large as can be expected from the free p-p and p-n cross sections. The shapes of the energy correlation spectra are quite different so that a direct comparison is difficult. It is conceivable that this result is unique to the particular angle pair chosen but this possibility is minimized by the fact that the (p,2p) angular correlation distribution is relatively flat in the vicinity of these angles and is not at a minimum. The tentative conclusion drawn is that the very large difference between the ^{6}Li(p,pn) and (p,2p) cross sections is related to the structure of ^{6}Li.

INADEQUACIES OF THE PWIA

The most obvious discrepancy between the PWIA and the data for ^{9}Be and ^{13}C is that the PWIA predicts cross sections many times too large, making it necessary to arbitrarily normalize the results of the calculation to the data in order to compare the shapes of the spectra. For these two targets, the absolute normalization factors were in the ranges of 30 to 50 and 25 to 40, respectively. This large attenuation of the cross section is due, at least in part, to the absorptive effects of the core nucleus. It is important to note that a single normalization factor for all angles would not bring the calculation into good

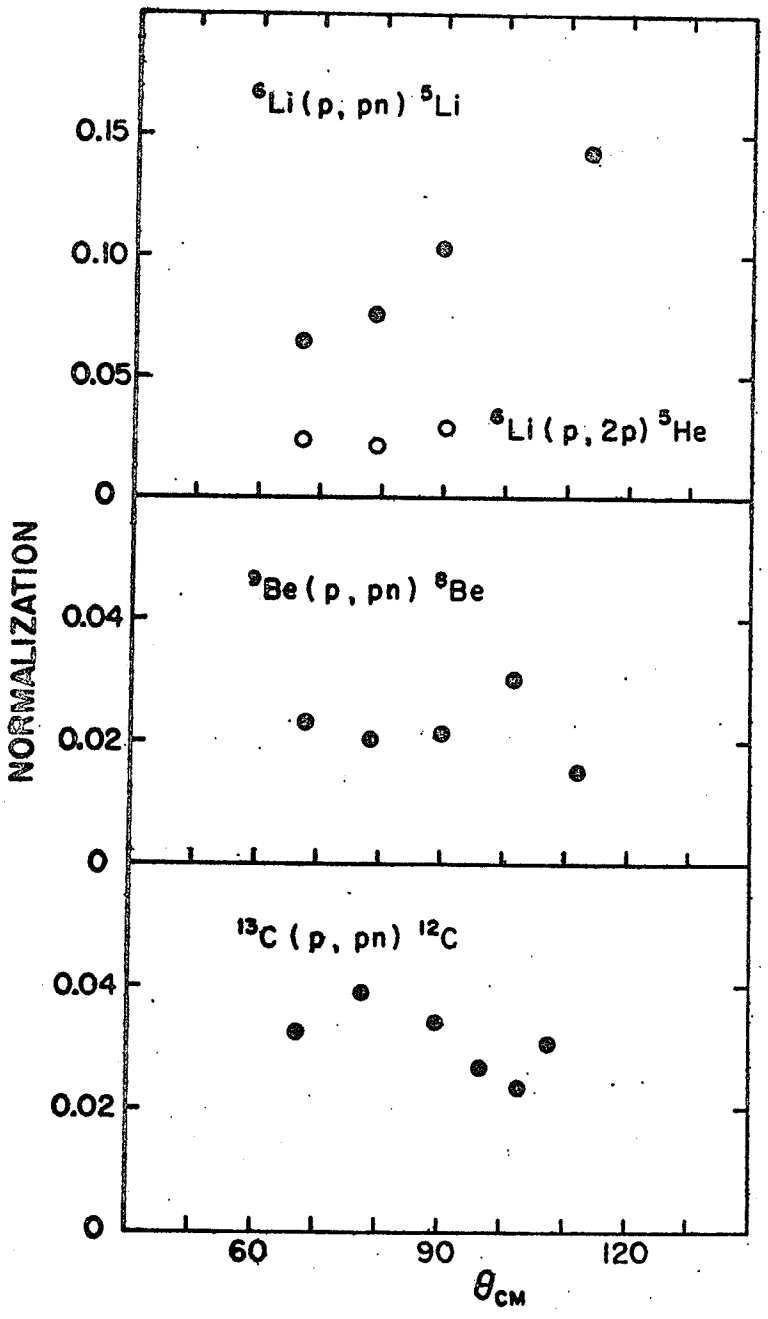

Fig. 3.17 Angular dependence of the normalization of the PWIA calculations presented in figures 3.13 and 3.15, as a function of the p-n cm scattering angle. For ^{13}C, results are included for one spectrum not shown in figure 3.15.

agreement with the data. Figure 3.17 shows the normalizations used in the calculations plotted as a function of the two-nucleon scattering angle in their centre of mass for the point of zero recoil momentum. ^{6}Li shows the previously-mentioned monotonic trend which is so similar to that of deuterium but ^{9}Be and ^{13}C have their own different variations.

The presence of strong absorptive effects of the core nucleus raises doubts that the RMS radii of the wave functions yeilding the best fits to the shapes of the spectra are meaningful. It is to be expected that the contribution to the knock-out cross section of that part of the spatial wave function lying inside the core nucleus will be suppressed relative to that extending outside. This means that the RMS radii of wave functions which fit the data are probably too large. Figure 3.18 shows the values obtained from the fits to the ^{9}Be and ^{13}C data compared with those obtained by Tyren et al (T66) from their 460 MeV (p,2p) measurements on a number of other nuclei. At that higher energy, absorption by the core is less important. The absissa is the binding energy of the valence nucleons in question. It can be seen that the present results for ^{9}Be and ^{13}C seem surprisingly large even for such small binding energies. Part of the very large difference in magnitude between the PWIA and the data can be attributed to the use of wave functions with excessively large RMS radii since such wave functions are more sharply peaked in momentum space and give rise to larger PWIA peak cross sections.

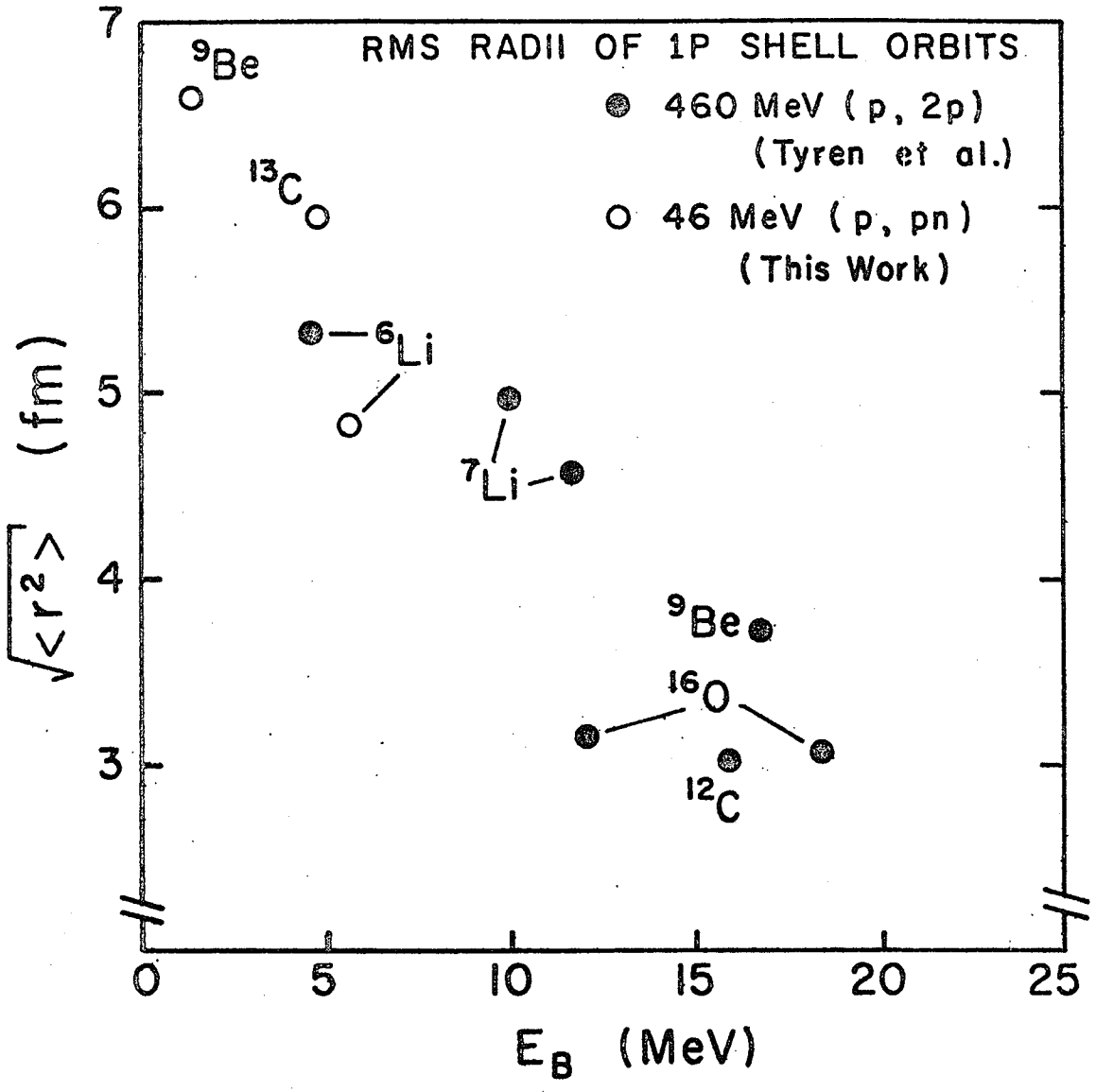

Fig. 3.18 The RMS radii of the 1p shell neutrons in ^{9}Be and ^{13}C obtained from the PWIA fits. They are compared with those of other 1p shell nuclei studied via the 460 MeV (p,2p) reaction (T66).

In view of these considerations, a natural question to arise is whether the use of optical model wave functions derived by fitting elastic scattering data will satisfactorily account for the absorptive and diffractive effects of the core nucleus for these knock-out reactions. If this were the case, it might be possible to obtain more reliable values for the RMS radii of the bound state wave functions. For these reasons, the distorted wave calculation described in the following chapter was undertaken.

4. THE DISTORTED WAVE IMPULSE APPROXIMATICN

THEORETICAL BACKGRCUND

To this point, the most comprehensive treatment that has been applied to the collisicn of two nucleons in the presence of a relatively massive core is the so-called Distorted Wave t-matrix Approximation (DWTA) (L66). In this formalism, the matrix element for the reaction ccnsisting of a particle with initial and final momenta $h\underline{k}_0$ and $h\underline{k}_2$ respectively knccking out a bound nucleon with final momentum $h\underline{k}_1$ is

$$T_\ell^m = A\iint \chi^{(-)*}(\underline{k}_1,\underline{r}_1)\,\chi^{(-)*}(\underline{k}_2,\underline{r}_2)\,t(\underline{r}_2-\underline{r}_1)\,\chi^{(+)}(\underline{k}_0,\underline{r}_2)\,\psi_\ell^m(\underline{r}_1)\,d^3\underline{r}_1\,d^3\underline{r}_2 \quad .. 4.1$$

"A" is an anti-symetrization operator which is applied if the two nucleons are identical, the χ's are distorted waves calculated from optical model potentials determined from elastic scattering, ψ_ℓ^m is the initial bound state wave function of the ejected nucleon and $t(\underline{r})$ is the two-nucleon t-matrix which is approximated by a central local pseudopotential. (Calculations have also been done with a non-local t-matrix.) The predictions of this approximation have been ccmpared with data from (p,2p) reactions at 50 MeV acquired in a symmetric coplanar detector qecmetry. Only the cross section for equal energy sharing of the two protons has been computed. Target nuclei investigated have included three in the 1p shell.. ^{12}C, ^{14}N, and ^{16}O as well as ^{40}Ca and ^{89}Y. Success in fitting the data has been quite limited. It has been noted that the fits

tend to improve with decreasing binding energy of the ejected proton (J71).

The approximation of the t-matrix by a central pseudopotential is appropriate only for situations where the singlet interaction dominates because it is mainly central. Such a situation is provided by the (p,2p) reaction at symmetric angles and energies because, at least in the absence of distortions, the p-p scattering is at 90° in the centre of mass of the two protons where triplet scattering is forbidden by the exclusion principle. Conversely, p-n scattering is dominated by the triplet interaction which is mainly tensor. This brings into question the advisability of attempting to fit (p,pn) cross sections with the above theory.

There is also a practical problem associated with extending the DWTA to the calculation of energy correlations at a variety of angles. Such calculations involve at least an order of magnitude more numerical computation than symmetric angular correlations because the optical model wave functions and radial overlap integrals (c.f. below) must be recomputed for each point in each energy correlation spectrum. Facilities for computations of this magnitude were not available at the University of Manitoba.

For these reasons it is necessary to consider a simplification of the DWTA. One that has been used for both (p,2p) and (p,p') at 150 MeV is the zero-range approximation. In order to invoke this approximation, the distorted waves are represented as products of plane waves and distortion factors.

$$\chi^{\pm}(\underline{k},\underline{r}) = D(\underline{k},\underline{r})\, e^{\pm i\underline{k}\cdot\underline{r}} \qquad 4.2$$

Also, a coordinate transformation is introduced.

$$\begin{aligned} \underline{r} &= \underline{r}_2 - \underline{r}_1 \\ \underline{r}' &= \underline{r}_1 \end{aligned} \qquad 4.3$$

For the (p,pn) reaction, the matrix element then becomes

$$T_\ell^m = \iint D(\underline{k}_1,\underline{r}')\, e^{-i\underline{k}_1\cdot\underline{r}'}\, D(\underline{k}_2,\underline{r}+\underline{r}')\, e^{-i\underline{k}_2\cdot(\underline{r}+\underline{r}')}$$
$$t(\underline{r})\, D(\underline{k}_0,\underline{r}+\underline{r}')\, e^{i\underline{k}_0\cdot(\underline{r}+\underline{r}')}\, \psi_\ell^m(r')\, d^3\underline{r}\, d^3\underline{r}' \qquad 4.4$$

Now, in the zero-range approximation, the distortion factors are assumed to vary sufficiently slowly as a function of $\underline{r}$ over the range of that variable where $t(\underline{r})$ is significant that they may be evaluated at $\underline{r}'$ instead of $\underline{r}'+\underline{r}$. When this is done and the exponential functions are re-arranged, we have

$$T_\ell^m = \iint e^{-(\underline{k}_2-\underline{k}_0)\cdot\underline{r}}\, t(\underline{r}) \quad D(\underline{k}_1,\underline{r}')\, e^{-i\underline{k}_1\cdot\underline{r}'}$$
$$D(\underline{k}_2,\underline{r}')\, e^{i\underline{k}_2\cdot\underline{r}'}\, D(\underline{k}_0,\underline{r}')\, e^{i\underline{k}_0\cdot\underline{r}'}\, \psi_\ell^m(\underline{r}')\, d^3\underline{r}\, d^3\underline{r}' \qquad 4.5$$

Then the double integral can be factored into two integrals, the first of which is the nucleon-nucleon scattering amplitude, T_{NN}. Finally, the reaction matrix element is

$$T_\ell^m = T_{NN} \int \chi^-(\underline{k}_1,\underline{r}')\, \chi^-(\underline{k}_2,\underline{r}')\, \psi_\ell^m(\underline{r}')\, \chi^+(\underline{k}_0,\underline{r}')\, d^3\underline{r}' \qquad 4.6$$

The cross section is proportional to the absolute square of T_ℓ^m, the first factor of which, $|T_{NN}|^2$, is related to the

experimental two body cross section. This is called the Distorted Wave Inpulse Approximatien (DWIA). The energy at which the two-body cross sectien is evaluated is subject to the same ambiquity as in the PWIA.

The energy range of validity of the DWIA as applied to the $^{12}C(p,2p)$ reaction has been determined by Lim and McCarthy (L66). Figure 4.1 shows their comparison of the DWIA and DWTA for this reaction at various incident energies. The obvious conclusion is that it is invalid at 50 MeV. However, there is reason to suspect that this result may not be directly applicable to the (p,pn) reaction on targets much more lightly bound than ^{12}C. A rough criterion for the validity of the zero-range approximation is the relative sizes of the nucleon-nucleon interaction range and the wavelength of the nucleons. The triplet effective range which dominates n-p scattering is about 40% less than the singlet effective range which dominates p-p scattering. A 40% difference in wavelength is a factor of two in energy. Also, the wave functions of more lightly bound valence nucleons extend spatially further outside the distorting potential where the incoming and outgoing wave functions are plane waves. As the factorizatien of eqn. 4.1 is exact for plane waves, the accuracy of the approximation can be expected to improve with such targets. If nothing else, these qualitive consideratiens indicate that calculations using the DWIA are worth attempting for these reactions in view of the difficulties associated with improving upon it.

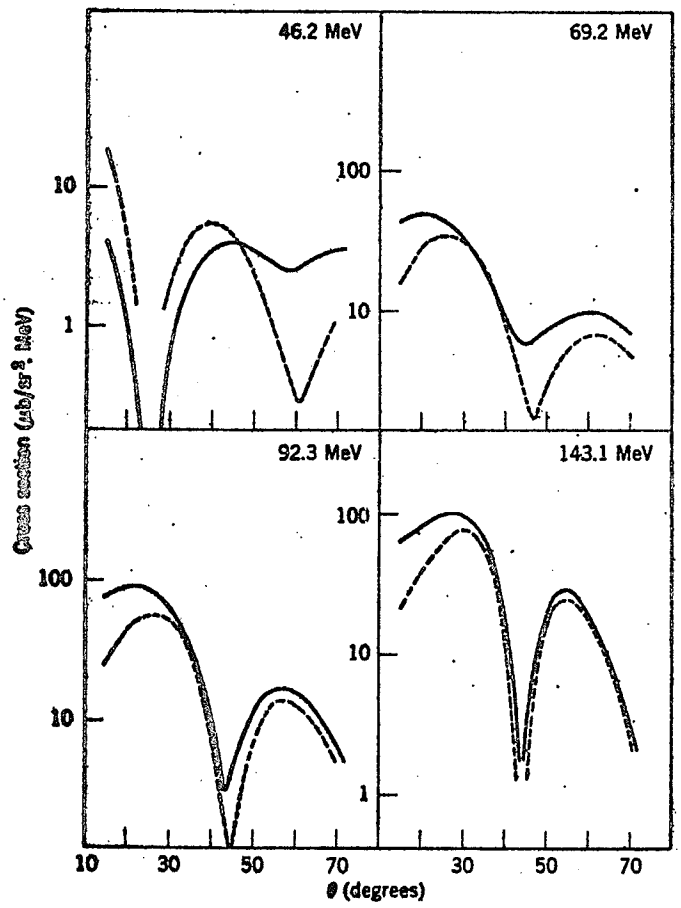

Comparison of the DWIA (dashed line) with the DWTA (solid line) at various energies for singlet (p, 2p) events in the reaction $^{12}C(p, 2p)^{11}B(1p$ state).

Fig. 4.1 Reproduction of a figure from (L66).

DETAILS OF THE CALCULATION

The calculations were performed following for the most part the detailed prescriptions of Jackson and Berggren (J65). Only a synopsis of definitions and results will be presented here. It should be noted that the symbology of eqns. 4.1 through 4.6 is different from that below in order that those expressions could be written as simply as possible. More specifically, the χ's and ψ_ℓ^m are functions of different (but related) coordinates in the following. For practical reasons, these wave functions are computed as a function of relative coordinates $\underline{r}_{oc} = \underline{r}_o - \underline{r}_c$, $\underline{r}_{1c} = \underline{r}_1 - \underline{r}_c$ and $\underline{r}_{oA} = \underline{r}_o - \underline{r}_A$. This is because the potentials to be included in the computations are most conveniently expressed as functions of these relative coordinates. The (different) labelling conventions for particles and momenta are shown in the diagram. The incident and ejected nucleons are numbered "0" and "1" respectively while the target and residual nuclei are labelled "A" and "C".

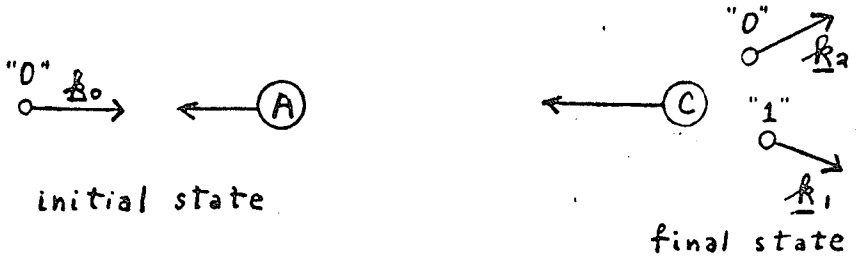

In order to derive equations through which the above wave functions may be calculated, it is necessary to express the Hamiltonians for the initial and final states in terms of the kinetic energy operators associated with momenta conjugate to the above relative coordinates. It is shown by Jackson and

Bergqren that the momenta conjugate to $\underline{r}_{oA}$, $\underline{r}_{ic}$, and $\underline{r}_{oc}$ are $\underline{k}_o$, $\underline{k}_1$, and $\underline{k}_2$, the momenta in the centre of mass of the whole system. It is also shown that Schrodinger's equation for the initial and final states can therefore be written as follows. For the initial state, the equation for the total system factorizes trivially to produce

$$\left[-\frac{\hbar^2}{2\mu_{oA}} \nabla_{oA}^2 + V_o(|\underline{r}_{oA}|) \right] \chi^+(\underline{r}_{oA}) = \frac{\hbar^2 k_o^2}{2\mu_{oA}} \chi^+(\underline{r}_{oA}) \qquad 4.7$$

for the incoming distorted wave and

$$\left[-\frac{\hbar^2}{2\mu_{ic}} \nabla_{ic}^2 + \overline{V}_1(|\underline{r}_{ic}|) \right] \Psi(\underline{r}_{ic}) = \epsilon_1 \Psi(\underline{r}_{ic}) \qquad 4.8$$

for the bound state of the ejected nucleon where ϵ_1 is the (negative) Q-value. μ_{oA}, for example, is the reduced mass $(1/m_o + 1/m_A)^{-1}$. V_o is the optical model potential and $\overline{V}_1$ is the potential initially binding the ejected nucleon to the core. For the final state, there is no exact factorization. As is pointed out in reference (J65), there will appear a coupling term in the equation for the total system associated with either the potential or kinetic energy, depending on the coordinates chosen. With the present choice, it is in the kinetic energy operator. Schrodinger's equation for the final state particles is

$$\left[-\frac{\hbar^2}{2\mu_{oc}} \nabla_{oc}^2 + V_o(|\underline{r}_{oc}|) - \frac{\hbar^2}{2\mu_{ic}} \nabla_{ic}^2 + V_1(|\underline{r}_{ic}|) - \frac{\hbar^2}{m_c} \underline{\nabla}_{oc} \cdot \underline{\nabla}_{ic} \right] \chi^-(\underline{r}_{oc}) \chi^-(\underline{r}_{ic})$$

$$= \left[\frac{\hbar^2 k_2^2}{2\mu_{oc}} + \frac{\hbar^2 k_1^2}{2\mu_{ic}} + \frac{\hbar^2 \underline{k}_2 \cdot \underline{k}_1}{m_c} \right] \chi^-(\underline{r}_{oc}) \chi^-(\underline{r}_{ic}) \qquad 4.9$$

As is suggested by Lim and McCarthy (L64), using rather

different notation, the coupling term can be treated as a perturbation if m_c is considerably larger than m_o and m_i so that $\nabla_{oc} \cdot \nabla_{ic}$ can be replaced by its eigenvalue, $-k_2 \cdot k_1$, thereby cancelling the corresponding term on the right. Then this equation is also separable.

$$\left[-\frac{\hbar^2}{2\mu_{oc}} \nabla_{oc}^2 + V_o(r_{oc})\right] \chi^-(r_{oc}) = \frac{\hbar^2 k_2^2}{2\mu_{oc}} \chi^-(r_{oc}) \qquad 4.10$$

and similarly for $\chi^-(r_{ic})$.

The overlap integral to be computed is

$$g_\ell^m = \iint \chi^{*-}(k_2, r_{oc})\, \chi^{*-}(k_1, r_{ic})\, \delta(r_{ic} - r_{oc})\, \chi^{+}(k_0, r_{oA})\, \psi_\ell^m(r_{ic})\, d^3 r_{ic}\, d^3 r_{oA} \qquad 4.11$$

Since $r_{oA} = r_{oc} - r_{ic}/m_A$,

$$g_\ell^m = \int \chi^{*-}(k_2, r)\, \chi^{*-}(k_1, r)\, \chi^{+}(k_0, ar)\, \psi_\ell^m(r)\, d^3 r \qquad 4.12$$

where $a = m_c/m_A$.

All the wave functions are expanded in partial wave series. Spin-orbit coupling is ignored for the optical model wave functions.

$$\psi_\ell^m = R_\ell(r)\, Y_\ell^m(\theta, \phi)$$

$$\chi^+(k_0, r) = \frac{1}{k_0 r} \sum_n i^{\sigma_n}\, i^{-n} \sqrt{4\pi(2n+1)}\; Y_n^0(\theta, \phi)\, F_n(k_0, r)$$

$$\chi^-(k_1, r) = \frac{1}{k_1 r} \sum_{p_1} i^{-\sigma_{p_1}}\, i^{p_1} \sqrt{4\pi(2p_1+1)} \sum_{\mu_1} Y_{p_1}^{\mu_1}(\theta, \phi)\, F_{p_1}(k_1, r)\, D_{\mu_1 0}^{p_1}(\theta_1, 0, 0) \qquad 4.13$$

$$\chi^-(k_2, r) = \frac{1}{k_2 r} \sum_{p_2} i^{-\sigma_{p_2}}\, i^{p_2} \sqrt{4\pi(2p_2+1)} \sum_{\mu_2} Y_{p_2}^{\mu_2}(\theta, \phi)\, F_{p_2}(k_2, r)\, D_{\mu_2 0}^{p_2}(\theta_2, \pi, 0)$$

σ_n, σ_{p_1} and σ_{p_2} are the coulomb phase shifts and the D's are rotation matrices.

When these expressions are substituted into the integral,

various properties of spherical harmonics are then used for simplification tc obtain tke fcrmula used in the computation.

$$g_\ell^m = (4\pi)^{3/2}\sqrt{2\ell+1}\sum_{p_1=0}^{\infty}\sum_{p_2=0}^{\infty}\sqrt{(2p_1+1)(2p_2+1)}\sum_{n=n_0}^{p_1+p_2+\ell} i^{(\sigma_n+\sigma_{p_1}+\sigma_{p_2})}\, i^{(n-p_1-p_2)}$$

$$U(\ell,n;p_1,p_2)\sum_{f=f_0}^{f_{max}}\frac{1}{2f+1}\,C(n,\ell,f;0,0)\,C(n,\ell,f;0,m)$$

$$\sum_{\mu=\mu_0}^{\min\{p_1,\,m+p_2}(-)^{m-\mu}\,C(p_1,p_2,f;\mu,m-\mu)\,Y_{p_1}^{\mu}(\theta_1,0)\,Y_{p_2}^{m-\mu}(\theta_2,0) \qquad \ldots 4.14$$

where $U(\ell,n;p_1,p_2)$ =

$$1/(k_0 k_1 k_2)\int F_n(k_0,ar)\,F_{p_1}(k_1,r)\,F_{p_2}(k_2,r)\,R_\ell(r)\,1/r\,dr$$

and the C's are Clebsch-Gordon coefficients whose symmetry properties determine the limitaticns cn tke summations over μ, f and n.

$$n_0 = \max\begin{cases}\ell-(p_1+p_2)\\ |p_1-p_2|-\ell\\ 0\end{cases} \qquad f_{max} = \min\begin{cases}n+\ell\\ p_1+p_2\end{cases}$$

$$f_0 = \max\begin{cases}|n-\ell|\\ |p_1-p_2|\\ |m|\end{cases} \qquad \mu_0 = \max\begin{cases}-p_1\\ m-p_2\end{cases} \qquad 4.15$$

Further such selection rules not shown abcve are that the sums $\ell+p_1+p_2+n$, p_1+p_2+f and $\ell+n+f$ mrst be even.

The convergence criterion used tc terminate the summations over p_1, p_2 and n was that the moduli cf two successive contributions to a summation be less than a specified fraction of the total accumulated sum to that pcint. This fraction was automatically scaled down for inner summations. Typical maximum

values for ^{9}Be(p,pn) were 26 for n and 18 for the p's. θ_1 and θ_2 are the angles of the final state particles in the centre of mass of the whole system.

The cross section in the laboratory is given by (L64)

$$\frac{d^3\sigma}{d\Omega_1 d\Omega_2 dT_1} = PSF \left(\frac{d\sigma}{d\Omega}\right)_{12} S \frac{N}{2J_A+1} \frac{1}{(2\pi)^3} \sum_{m=-l}^{l} W_m \left| g_l^m \right|^2 \qquad 4.16$$

where

$$W_m = \sum_{M_c=-J_c}^{J_c} \sum_{M_A=-J_A}^{J_A} \left[C(J_c, J_s, J_A; M_c, M_A - M_c)\, C(l, s, J_s; m, -m + M_A - M_c) \right]^2 \qquad 4.17$$

and

$$PSF = \frac{k_1 k_2^2 E_c E_{12cm}^2}{\hbar m_2 \left| k_2 E_c + E_2 (k_2 - k_0 \cos(\theta_2) + k_1 \cos(\theta_1 - \theta_2)) \right|} \qquad 4.18$$

is a kinematic factor including phase space density with the E's representing relativistic total energies. Use is made of the translational invariance of g_l^m so that these kinematic quantities are calculated in the labcratory. $\left(\frac{d\sigma}{d\Omega}\right)_{12}$ is the two-body cross section evaluated in the centre of mass of particles 0 and 1. S is the spectroscopic factor or reduced width amplitude denoting the probability of finding the target nucleus in the (core+ejected nucleon) configuration. N is the number of nucleons in the subshell of spin J_s and orbital angular momentum l from which particle 1 of intrinsic spin s is ejected. (J_A, M_A) and (J_c, M_c) are the angular momentum quantum numbers of the target and residual nuclei, respectively. It can be shown that $|g_l^m| = |g_l^{-m}|$ so that the computation of g_l^m need not be done for negative values of m.

The optical model wave functions were calculated using

techniques developed by Melkanoff et al. for the SEEK code (M66) for elastic scattering analysis. Woods-Saxon form factors were used for the potentials. The parameters were determined from the prescriptions of Watson et al (WSS69) who fitted elastic scattering of 10 to 50 MeV nucleons on all available 1p shell target nuclei. Their parameterizations are as follows.

$$V = 60.-.30E+.4Z/A \pm 27.0(N-Z)/A \text{ MeV}$$

$$W_S = .64E \pm 10.0(N-Z)/A, \quad E<13.8 \text{ MeV},$$

$$= 9.6-.06E \pm 10.0(N-Z)/A, \quad E \geq 13.8 \text{ MeV}$$

The + sign is for protons and the - sign is for neutrons.

$$W_V = 0, \quad E<32.7 \text{ MeV},$$

$$= 1.15(E-32.7), \quad 32.7 \leq E \leq 39.3 \text{ MeV},$$

$$= 7.5 \text{ MeV}, \quad E>39.3 \text{ MeV}.$$

$$r_C = r_R = r_I = 1.15-.001E \text{ f.}$$

$$a_R = .57 \text{ f.}$$

$$a_I = .50 \text{ f.}$$

E is the kinetic energy in the centre of mass.

The bound state wave function $R_\ell(r)$ was also computed in a Woods-Saxon potential with the diffuseness the same as $a_R = .57$ f. but with the radius a free parameter as discussed later. For a given well geometry, the well depth was varied until a bound state with the correct binding energy was obtained.

Computer time requirements for computation of energy correlation spectra consisting of approximately 12 energy values for each of 16 angle pairs was about 45 minutes on an IBM 360 model 65. This is strongly dependent on the binding energy of the ejected nucleon. The above set of angle pairs

were equally shared between ^{13}C and $^{9}Be(p,pn)$.

DWIA CALCULATIONS FOR ^{9}Be AND $^{13}C(p,pn)$

The solid curves on figures 4.2 and 4.3 are the predictions of the DWIA for these two reactions at all measured angle pairs. They are not arbitrarily normalized. The parameterization of the optical model potentials used for both initial and final states is unmodified from that given by Watson et al with the exception that the spin-orbit term is excluded. The discussion of the spectroscopic factors and bound state parameters used will be postponed until after the following discussion of parameter sensitivity.

The question of whether fitting the calculation to the data will determine a parameter used in the calculation can only be resolved by studying the relative sensitivity of the theory to all the input information. Even though, in principle, the optical model potentials are considered to be determined by elastic scattering, there are often ambiguities in this determination resulting from such factors as the insensitivity of the fits to the value of Vr^2. Using the Watson et al parameter set as a standard, several individual parameters were varied in the DWIA calculation to determine its sensitivity.

First, a rather large change in the optical potential depth and radius were made while keeping Vr^2 constant. r was increased by 20% and V was decreased by 44%. For both ^{9}Be and ^{13}C, little change resulted in either the shapes or the magnitudes for the various angle pairs relative to one another. There was a fairly uniform decrease in the over-all magnitudes

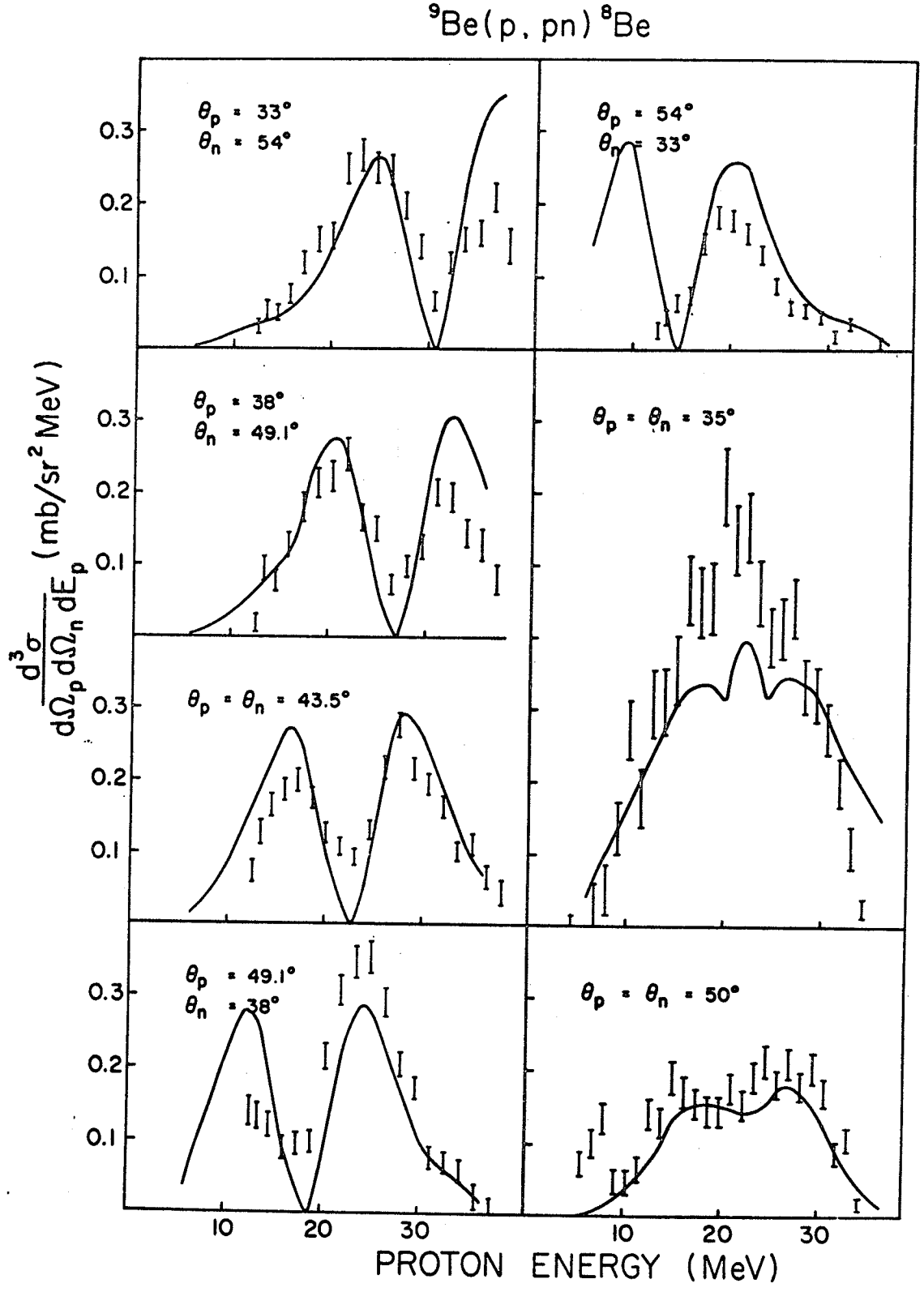

Fig. 4.2 The cross sections for ^{9}Be(p,pn)^{8}Be at 45.7 MeV. The solid curves are the results of the DWIA calculations with a spectroscopic factor of 1/3 (N×S=1) and a bound state RMS radius of 4.0 f.

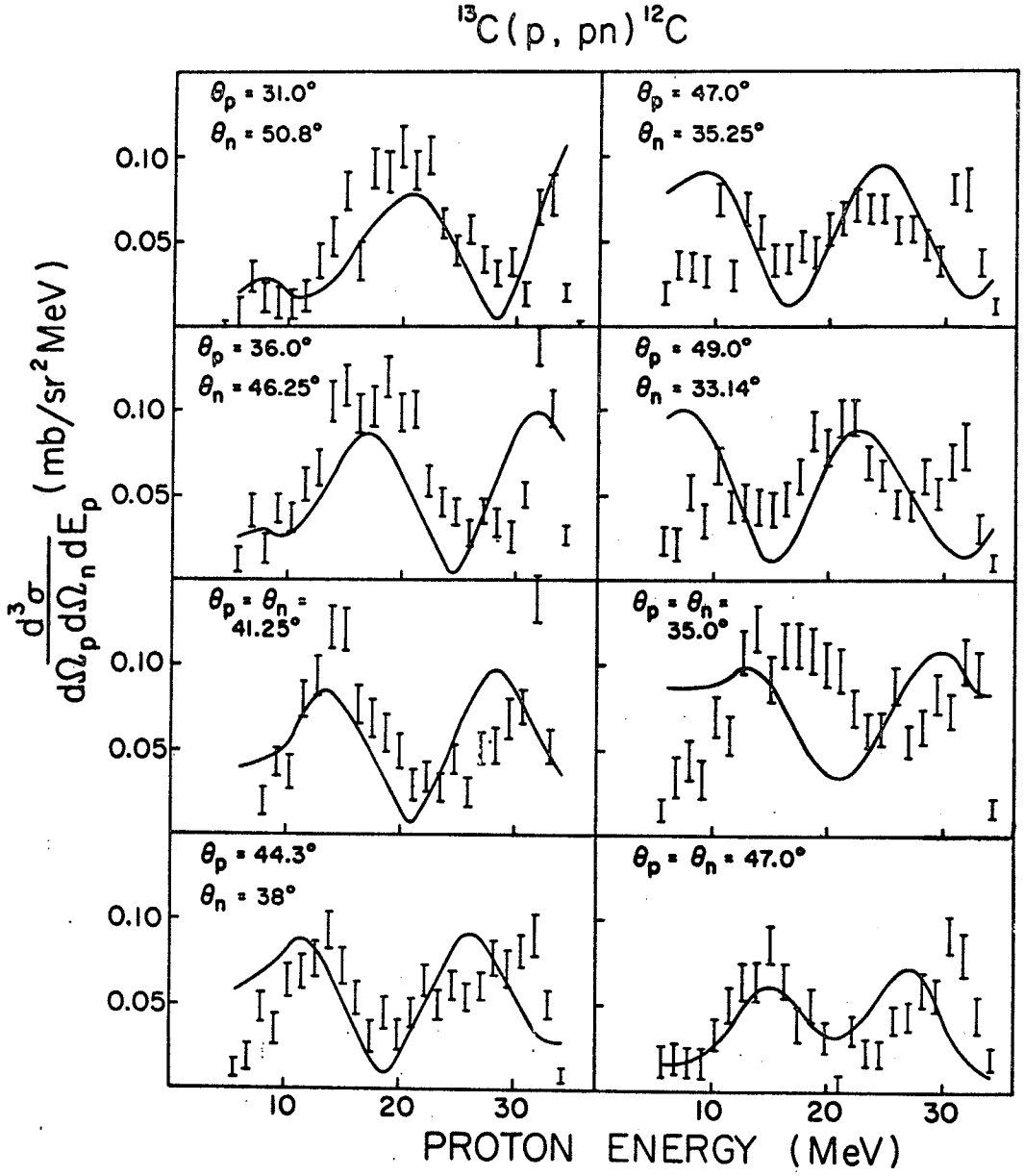

Fig. 4.3 The cross sections for $^{13}C(p,pn)^{12}C$ at 45.6 MeV. The solid curves are the results of the DWIA calculations with a spectroscopic factor of unity and a bound state RMS radius of 3.61 f.

of 10-15% for ^{9}Be and 40-45% for ^{13}C. Next, V alone was increased by 20%. This resulted in only small (5%) changes in the shapes of some of the spectra except for that of ^{9}Be at (35°,35°) which was decreased by 20% and the extreme tails of the ^{13}C curves which were attenuated. The general result could be characterized by saying that the fits to the shapes of the spectra were improved for ^{13}C and worsened for ^{9}Be. Finally, both the surface and volume imaginary potential strength was increased by 30%. This had no effect on the ^{9}Be results and almost none for ^{13}C except that the tails were again attenuated. The general conclusion that could be drawn from the optical model parameter study is that it is not possible to greatly improve the fits to the shapes of the spectra and that the over-all magnitude is sensitive only to the radius parameter.

The effects of varying the bound state parameters were also studied. Both the radius and diffuseness of this potential well were individually altered while the optical model parameters remained unchanged from those of Watson et al. The result can be stated very simply. Such alterations had very little effect on the shapes or relative magnitudes of the cross sections at the various angle pairs. Only the over-all magnitude of the cross sections was changed significantly. The magnitude was increased by an increase in either the radius or diffuseness of the bound state potential well. For the same change in RMS radius of the wave function, the cross section seemed to be more sensitive to the diffuseness than the radius.

In summary, the parameter studies indicate that DWIA calculations for the (p,pn) reaction on nuclei with such small neutron separation energies as ^{9}Be and ^{13}C predict cross sections that are fairly isotropic with angle. No reasonable variation of the optical model or bound state potential parameters will permit the theory to reproduce the angular dependence of the ^{9}Be experimental cross sections for asymmetric quasi-free angle pairs. For example, at the (proton,neutron) angle pair of (49.1°,38°), the theory is too small while at (54°,33°), it is too large. Also, no parameter variation significantly shifts the positions of the peaks of the cross sections in the energy correlation projections. In the plane wave theory, these peak positions are determined by the RMS radius of the bound state wave function. In this distorted wave theory, the results seem to depend mainly on how much of the bound state spatial wave function extends out past the distorting potential. Further, the only aspect of the results that is strongly affected is the over-all magnitude. This makes it difficult to determine the RMS radius of the bound state wave function by fitting the data because this parameter has much the same effect on the calculation as the spectroscopic factor which is also uncertain.

For the fits shown to the ^{13}C data, the bound state potential radius, r_B, was chosen to be 3.7 fermis. This is the value that yields the best fit using a spectroscopic factor, S, of unity. The data could be equally well fitted by a larger radius together wih a smaller value of S. However, the value of

r_B chosen is already somewhat larger than that obtained by scaling by $A_c^{1/3}$ the value of 3.5 f. used for a square well by Lim and McCarthy (L64) in their analysis of $^{12}C(p,2p)$ at 155 MeV (A_c is the mass of the core nucleus). Their choice is consistent with information about charge distributions from electron scattering. Further, the inclusion of a finite diffuseness in the present case is equivalent to the use of an even larger radius with a square well. The conclusion that can be drawn from these points is that either S is large or r_B is abnormally large. Cohen and Kurath (C67) have calculated a theoretical value for the spectroscopic factor of .61. Their calculation is based on effective interactions deduced by fitting experimental energy levels. Taketani et al (T68) obtain a value of .82 from their DWBA analysis of the $^{13}C(p,d)$ reaction for the transition to the ground state of ^{12}C. A value of unity is probably within their uncertainties. If we take this as an upper limit for S, a lower limit of 3.6 f. is set on the RMS radius of the $p_{1/2}$ neutron, provided, of course, that the DWIA is valid for this reaction as far as the prediction of cross section magnitudes is concerned. It is worth noting that a value of S of .75 can be accommodated with an RMS radius of 3.7 f. when a well radius and diffuseness of 3.0 and 1.0 f. are used. The 15% estimated uncertainty in the absolute magnitude of the $^{13}C(p,pn)$ cross sections can be translated into an uncertainty in RMS radius of approximately 5%. It is important to note that the values of RMS radii being given here represent the separation of the neutron and core rather than the neutron

and the centre of mass.

The curves shown for $^{9}Be(p,pn)$ in figure 4.2 were computed with a spectroscopic factor of 1/3 and a bound state radius of 3.0 f. which is close to the result of scaling the ^{12}C value by $A_C^{1/3}$. The corresponding RMS radius is 4.0 f. It should be noted that the definition of of spectroscopic factor being used here does not include the number of neutrons, N, in the outer subshell. This number is 3 in the case of ^{9}Be and is included separately in the expression for the cross section. Because of the very small neutron and alpha-particle separation energies for this nucleus, it is tempting to consider it in terms of a alpha-alpha-neutron cluster structure. This would be consistent with the spectroscopic factor of 1/3 which means that there is effectively only one neutron available to be knocked out. However, Cohen and Kurath predict an even smaller value of .58 for the product of N and S. Using this value, a set of bound state parameters that will fit the magnitude of the data is a radius and diffuseness of 3.0 and 1.0 f. with an RMS radius of 4.63 f.

Finally, in figure 4.4, the DWIA calculation is compared with the $^{12}C(p,pn)$ data at the one angle pair at which the measurement was made. The radius and diffuseness of the bound state well were taken to be 3.5 and .57 f. with a resultant RMS radius of 2.83 f. S is given a value of .4 in order to normalize the calculation to the data but the proton-neutron interaction is so far off the energy shell with this target that the on-shell approximation makes the magnitude of the

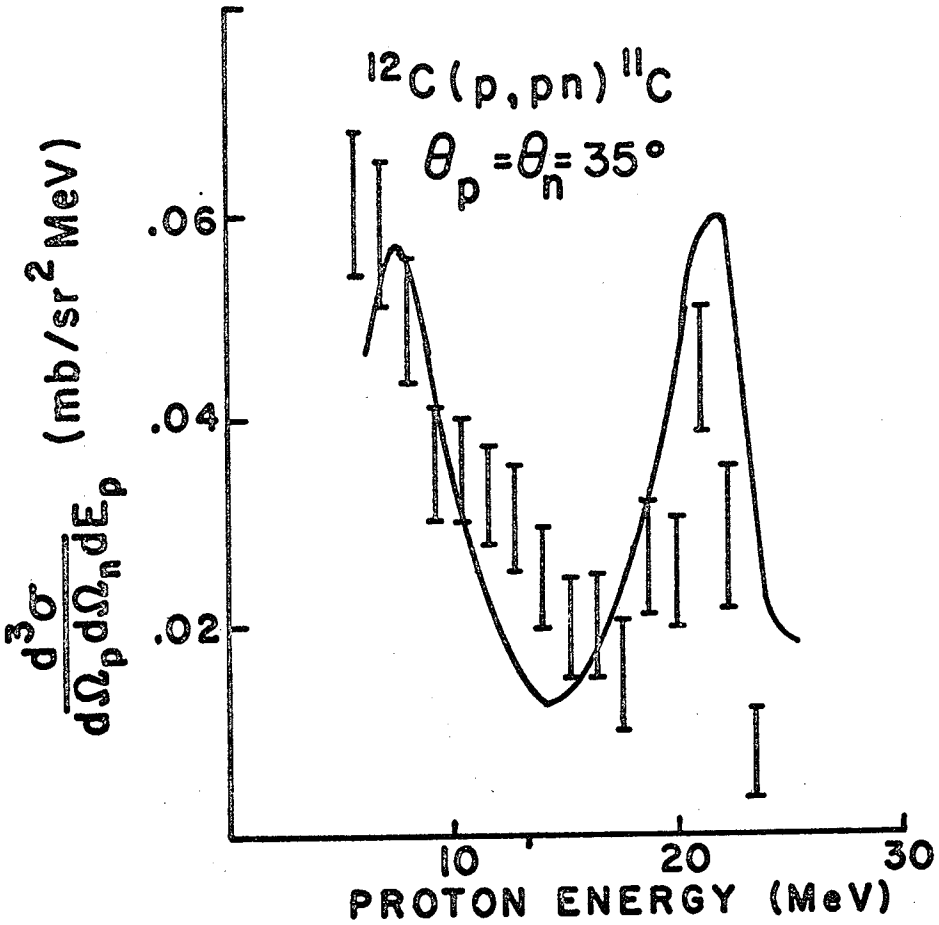

Fig. 4.4 The cross sections for the $^{12}C(p,pn)^{11}C$ reaction at 45.6 MeV at the detector angles indicated. The solid curve is the result of the DWIA calculation with a spectroscopic factor of .4 (NxS=1.6) and a bound state radius of 2.83 f.

calculation uncertain. Although the fit to the shape is fair, there is probably neither sufficient experimental data nor confidence in the calculation for this target to justify an attempt to draw conclusions concerning characteristics of the bound state. One point that can be made is that the calculation does not seem to show any of the asymmetry that seems to be present in the data.

DWIA calculations were not attempted for the reactions on ^{6}Li because of the importance of the previously-discussed s-state admixture in this nucleus. The associated complexities involving the unbound residual nucleus are not easily incorporated in the DWIA.

5. SUMMARY AND CONCLUSIONS

The (p,pn) reaction on four 1p shell nuclei, ^{6}Li, ^{9}Be, ^{13}C and ^{12}C, as well as the ^{6}Li(p,2p) reaction have been studied at 46 MeV. A number of suprising features have been found. In the case of ^{6}Li, the (p,pn) cross sections are about four times those for (p,2p). Also, the (p,pn) data at quasi-free angles show a marked angular dependence not observed with (p,2p). However, the shapes of the projections of the energy correlation spectra are quite similar for the two reactions and show the strong s-state component previously observed at higher energies. The cross sections for ^{9}Be and ^{13}C also show significant angular dependence although it is qualitatively different from and not as dramatic as that of ^{6}Li(p,pn). At one pair of angles, the cross section for (p,pn) on ^{12}C was found to be somewhat larger than for (p,2p) although the difference is much smaller than that observed for ^{6}Li. The shapes of the projections are quite different for the two reactions.

The data were compared with the Plane Wave Impulse Approximation which, not unexpectedly, was found inadequate in several respects. Most notably, a single renormalization to take account of absorption does not bring it into agreement with the data. Also, RMS radii of bound state wave functions giving the best fit to the shapes of the spectra are unrealistically large. These discrepancies are attributed to the absorptive and diffractive effects of the core nucleus.

An attempt was made to take account of these effects by means of a zero-range distorted wave calculation. For ^{9}Be and ^{13}C, this calculation was found to be very sensitive to the RMS radius of the bound state wave function of the ejected neutron. However, it is only the overall magnitude of the results that is significantly affected so that the determination of the RMS radius from the fits is only as reliable as the values used for the spectroscopic factors for the reactions. The quality of the fits to the shapes and angular dependence of the cross sections is not greatly affected by the adjustment of any parameter of the calculation.

A conclusion that can be drawn from the present studies is that the (p,pn) reaction, especially when studied at various asymmetric quasi-free angles, is useful for revealing reaction mechanism complexities that tend to be masked with the (p,2p) reaction at symmetric angles because of the symmetries imposed on the cross sections by the identical particles in the final state. This capability of the (p,pn) reaction was first exploited by Peterson et al (P70,P71) in their studies of deuterium. In the present work, all of the targets investigated with this reaction resulted in cross sections which showed significant asymmetries both in their dependence on angle and in the energy correlation projections. It is particulaly significant that distorted wave calculations show no tendency at all to imitate this behaviour although, in other respects, the fits are fair. This inadequacy is taken to mean that, even with a target such as ^{13}C with the desirable spectroscopic

configuration of a single nucleon relatively lightly bound to a core with a closed subshell, and especially with ^{9}Be and ^{6}Li, there are significant departures from what Lim and McCarthy call the "Quasi-three body assumption" (L66). In other words, optical model potentials do not seem to adequately describe the effects of the presence of the core nucleus.

REFERENCES

B64 B.M. Bardin and M.E. Rickey, Rev. Sci. Instr. 35,902 (1964)

B72 K.H. Bray, M. Jain, K.S. Javaraman, G. LoBianco, G.A. Moss, W.T.H. van Oers, D.O. Wells and F. Petrovich, Nucl. Phys. A189,35 (1972)

C67 S. Cohen and D. Kurath, Nucl. Phys. A101,1 (1967)

E55 Robley D. Evans, "The Atomic Nucleus", 785, Mcgraw-Hill Book Company (1955)

E72 Electronic Space Products Inc., 854 South Robertson Blvd., Los Angeles Cal 90035

E73 S. Elbaker, private communication

G62 J.P. Garron, J.C. Jacmart, M. Riou, C. Ruhla, J. Teillac and K. Strauch, Nucl. Phys. 37,126 (1962)

G70 P. Gaillard, M. Chevallier, J.Y. Grossiord, A. Guichard, M. Gusakow and J.R. Pizzi, Phys. Rev. Lett. 25,593 (1970)

J65 Daphne F. Jackson and Tore Berggren, Nucl. Phys. 62,353 (1965)

J66 Gerhard Jacob and Th. A.J. Maris, Rev. Mod. Phys. 38,121 (1966)

J70 M. Jain, P.G. Roos, H.G. Pugh and H.D. Holmgren, Nucl. Phys. A153,49 (1970)

J71 J. Janiszewski and I.E. McCarthy, The Flinders University of South Australia Preprint FUPH-12-53 (Oct. 1971)

J73 Gerhard Jacob and Th. A.J. Maris, Rev. Mod. Phys. 45,6 (1973)

L64 K.L. Lim and I.E. McCarthy, Phys. Rev. 133,B1006 (1964)

L66 K.L. Lim and I.E. McCarthy, Nucl. Phys. 88,433 (1966)

M66 M.A. Melkanoff, T. Sawada and J. Raynal, University of California at Los Angeles Report No. 66-10, unpublished

M68 I.E. McCarthy, "Introduction to Nuclear Theory", 491, John Wiley & Sons, Inc., New York (1968)

M69 M. Martini and T.A. McMath, Nucl. Instr. 76,1 (1969)

M70 D.J. Margaziotis, G. Paic, J.C. Young, J.W. Verba, W.J. Braithwaite, J.M. Cameron, D.W. Storm and T.A. Cahill, Phys. Rev. C2,2050 (1970)

M72 I.A. Mackenzie, S.K. Mark and Tseh Y. Li, Nucl. Phys. A195,609 (1972)

N71 Nuclear Enterprises, Inc., 935 Terminal Way, San Carlos, Cal 94070

P65 H.G. Pugh, D.L. Hendrie, Marc Chabre and E. Boschitz, Phys. Rev. Lett. 14,434 (1965)

P67 H.G. Pugh, D.L. Hendrie, Marc Chabre, E. Boschitz and I.E. McCarthy, Phys. Rev. 155,1054 (1967)

P69 J.R. Pizzi, M. Gaillard, P. Gaillard, A. Guichard, M. Gusakow, G. Reboulet and C. Ruhla, Nucl. Phys. A136,496 (1969)

P70 E.L. Peterson, R.G. Allas, R.O. Bondelid, A.G. Peiper and R.B. Theus, Phys. Lett. 31B,209 (1970)

P71 E.L. Peterson, R.G. Allas, R.O. Bondelid, D.I. Bonbright, A.G. Pieper and R.B. Theus, Phys. Rev. Lett. 27,1454 (1971)

P72 Penn Spectra-Tech, Inc., 411 Bickmore Dr., Wallingford, Pa 19086

R67 J.C. Roynette, M. Arditi, J.C. Jacmart, F. Mazloum, M. Riou and C. Ruhla, Nucl. Phys. A95,545 (1967)

S66 I.S. Shapiro, Proc. Int. School Physics, "Enrico Fermi", Varenna, XXXVIII, 210, Academic Press, New York (1966)

S71 Noel R. Stanton, "A Monte Carlo Program for Calculating Neutron Detector Efficiencies in Plastic Scintillators", Ohio State University Preprint C00-1545-92 (Feb. 1971)

Sa68 Sakae Saito, Jun Hiura and Hajime Tanaka, Prog. Theor. Phys. 39,635 (1968)

Sh68 I.S. Sherman, R.G. Roddick and A.J. Metz, IEEE Trans. Nucl. Sci. NS-15,500 (1968)

T66 H. Tyren. S. Kullander, O. Sundberg, R. Ramachandran, P. Isacsson and T. Berqgren, Nucl. Phys. 79,321 (1966)

T68 H. Taketani, J. Muto, Y. Yamaguchi and J. Kokame, Phys. Lett. 27B,625 (1968)

V67 J.W. Verba, H. Willmes, R.F. Carlson, I. Slaus, J. Reginald Richardson and E.L. Peterson, Phys. Rev. 153,1127 (1967)

W69 J.W. Watson, thesis, Univ. of Md. (1969)

W71 J.W. Watson, H.G. Pugh, P.G. Roos, D.A. Goldberg, R.A.J. Riddle and D.I. Bonbright, Nucl. Phys. A172,513 (1971)

WSS69 B.A. Watson, P.P. Singh and R.E. Segel, Phys. Rev. 182,977 (1969)